

1 **Transferability of machine learning-based modeling frameworks across flood events**
2 **for hindcasting maximum river water depths in coastal watersheds**

3 Maryam Pakdehi^{1,2}, Ebrahim Ahmadisharaf^{1,2*}, Behzad Nazari³, Eunsuem Cho^{1,2}

4
5 ¹Department of Civil and Environmental Engineering, FAMU-FSU College of Engineering,
6 Tallahassee, FL 32310

7 ²Resilient Infrastructure and Disaster Response Center, FAMU-FSU College of Engineering,
8 Tallahassee, FL 32310

9 ³Department of Civil Engineering, University of Texas at Arlington, Arlington, TX 76010

10
11 ***Corresponding Author:**

12 Dr. Ebrahim Ahmadisharaf

13 Research Faculty I

14 Department of Civil and Environmental Engineering

15 Resilient Infrastructure and Disaster Response Center

16 FAMU-FSU College of Engineering

17 Tallahassee, FL 32310, USA

18 Tel: +1 716-803-5498

19 Emails: eahmadisharaf@eng.famu.fsu.edu and eascesharif@gmail.com

20 **Abstract**

21 Despite applications of machine learning (ML) models for predicting floods, their transferability
22 for out-of-sample data has not been explored. This paper developed an ML-based model for
23 hindcasting maximum river water depths during major events in coastal watersheds and evaluated
24 its transferability across other events (out-of-sample). The model considered spatial distribution of
25 influential factors, which explain the underlying physical processes, to hindcast maximum river
26 water depths. Our model evaluations in a six-digit hydrologic unity code (HUC6) watershed in
27 Northeastern US showed that the model satisfactorily hindcasted maximum water depths at 116
28 stream gauges during a major flood event, Hurricane Ida (R^2 of 0.94). The pre-trained, validated
29 model was successfully transferred to three other major flood events, Hurricanes Isaias, Sandy,
30 and Irene ($R^2 > 0.70$). Our results showed that ML-based models can be transferable for
31 hindcasting maximum river water depths across events when informed by the spatial distribution
32 of pertinent features, their interactions and underlying physical processes in coastal watersheds.

33 **Keywords**

34 Flood modeling; Hindcasting; Machine learning algorithms; Maximum flood depth; Model
35 transferability; Coastal watersheds.

36 **1. Introduction**

37 Floods can damage civil infrastructure, business disruptions, and environmental degradation.
38 Mitigation strategies are planned and implemented to mitigate these damages. To propose effective
39 protection strategies, predictive models are used to evaluate watershed responses under various
40 plausible flood scenarios (Fernández-Pato et al. 2016; Kundzewicz et al. 2019; Viglione et al.
41 2014). These models are essential tools to inform decision makers about suitable risk management

42 strategies and actions. Flood models can be broadly categorized as physically-based, morphologic-
43 based and data-driven.

44 Physically-based models, widely used for predicting hydrologic events, are considered
45 reliable tools for assessing different flood scenarios (Fernández-Pato et al. 2016). These models
46 solve the shallow water equations to derive flood characteristics. Developing physically-based
47 models requires certain meteorologic, hydrologic, and geomorphologic data. If these data are not
48 available at the desired scale, such models cannot be developed. For instance, global inundation
49 models are available to model flooding across the world, but they may not be efficient for small
50 scale applications. In such instances, data-driven models can be a flexible alternative as they can
51 adapt to varying levels of data availability by focusing on the features with sufficient data. This
52 flexibility remains one of the advantages of data-driven models over physically-based models.
53 Physically-based models also need significant computational resources, especially in the case of
54 high-resolution, multidimensional (2D and 3D) or stochastic models that necessitate numerous
55 simulations. To enhance the speed of flood simulations, techniques such as parallel computing,
56 graphics processing units (GPUs), and simplified models have been utilized (Costabile, Costanzo,
57 and Macchione 2017; Kalyanapu et al. 2011; Ming et al. 2020; Sridhar, Ali, and Sample 2021;
58 Zahura et al. 2020). However, resources for utilizing these approaches are not always available
59 (Zhang et al. 2014).

60 Morphologic-based models, which approximate flat-water surfaces over small spatial scales,
61 are also used for flood predictions (Bates 2022). Bathtub (Anderson et al. 2018; Kulp & Strauss
62 2019) and height above nearest drainage (HAND; Rennó et al. 2008) are two widely used models
63 in this modeling category. Jafarzadegan and Merwade (2019) used a probabilistic function based
64 on HAND, computed from a digital elevation model (DEM), and optimized it for accuracy, to

65 delineate 100-year floodplains. Zheng et al. (2018) developed a synthetic rating curve using the
66 HAND method, which represents river water depth measurements, similar to hydraulic models or
67 stream gauge readings. While these models are computationally efficient, they can overestimate
68 flooded area and are limited to the number of features they use; these models rely on topographic
69 data (Bates 2022; Bates et al. 2005) and tend to work well only in confined valleys. The sole use
70 of topographic data makes HAND-based models impractical for low-lying areas, especially coastal
71 watersheds that experience a combination of hydrologic and oceanic processes (e.g., tidal
72 influences, storm surges and wave action); other flood influencing factors, which represent such
73 overlooked underlying physical processes, are needed along for predictions in such watersheds.
74 Coastal regions also experience a combination of oceanic and hydrologic processes, which might
75 not be fully represented by HAND. Both HAND-based and bathtub models are limited in
76 representing such terrains as they might not fully capture the intricate interactions between oceanic
77 and hydrologic factors in coastal areas. Consequently, in coastal watersheds, where unconfined
78 floodplains and complex interactions are prevalent, alternative modeling approaches that consider
79 a broader range of factors are crucial for producing reliable flood predictions. Incorporating these
80 overlooked underlying physical processes becomes essential in providing comprehensive flood
81 predictions in these intricate environments.

82 ML and, in particular, deep learning (DL) models, offer an alternative approach that can rapidly
83 capture complex relationships between various influencing factors and flood characteristics. ML
84 models have the potential to provide satisfactory flood predictions (Mishra et al. 2022). Such data-
85 driven models have gained popularity in overcoming the limitations of physically-based and
86 morphologic-based models in flood modeling (Khosravi et al. 2018). These models
87 mathematically represent the nonlinearity of flood dynamics with pertinent features and observed

88 flood data using complex nonlinear structures and algorithms. Data-driven models have been
89 found as promising tools due to their quick development time and minimal input requirements
90 (Guo et al. 2021; Löwe et al. 2021; Zahura et al. 2020). Example data-driven models for flood
91 predictions include multiple linear regression, artificial neural networks (ANNs), random forest,
92 support vector machine, and support vector regression models (Adamowski et al. 2011; Kim et al.
93 2016; Rafiei-Sardooi et al. 2021; Rahmati et al. 2016; Rezaie et al. 2022; Wang et al. 2015;
94 Youssef et al. 2022). While there are several issues with these models, including interpretability,
95 techniques such as SHapley Additive exPlanations (SHAP) can enhance understanding of these
96 models' decision-making processes (Lundberg and Lee 2017; Abdollahi and Pradhan 2021). These
97 models enable the identification of key features that drive flood characteristics.

98 Previous research has shown that various ML algorithms are effective in predicting flood
99 extents and generating susceptibility maps, with a focus on classification ML models (Khosravi et
100 al. 2018; Rahmati et al. 2016; Rezaie et al. 2022; Youssef et al. 2022). However, these studies have
101 limitations in terms of their experimental design and scope. For instance, some of these studies
102 created datasets of flooded and unflooded points using remote sensing. The datasets were often
103 split into two subsets, and ML models were examined trained on a portion of the dataset (training
104 set) and then tested for the remainder of the dataset (validation or test set). This approach helps in
105 identifying the most effective models for flood predictions based on performance metrics, such as
106 recall or the area under the Receiver Operating Characteristic (ROC) curve. Another limitation of
107 these ML studies is the reliance on a single event for training and validation. As such, it is unclear
108 whether a trained and validated model can satisfactorily predict other flood events. These
109 limitations call for studies that evaluate more complex methodologies and a broader range of
110 scenarios on the effectiveness of ML algorithms for predicting flood characteristics. These

111 limitations call for studies that evaluate more complex methodologies and a broader range of
112 scenarios on the effectiveness of ML algorithms for predicting flood characteristics.

113 Another application of ML models for flood inundation prediction has been coupling them
114 with physically-based models for improving their performance. Such applications are based on the
115 hybrid use of ML and physically-based modeling categories. For instance, Chang et al. (2022)
116 suggested an approach that incorporated principal component analysis(PCA), self-organizing
117 maps, and nonlinear autoregressive models with exogenous inputs to mine spatiotemporal data and
118 forecast regional flood inundation. The authors recognized the value of using ML algorithms
119 together with a 2D hydraulic model to simulate urban flood inundation considering different
120 rainfall events. Elkhachy (2022) developed a hybrid approach to predict flash flood depths
121 combining 2D hydraulic modeling with ML algorithms; water depths simulated by the Hydrologic
122 Engineering Center's River Analysis System (HEC-RAS; Brunner 2016) model served as training
123 and test datasets for ML algorithms. Löwe et al. (2021) trained an ANN model to identify patterns
124 in rainfall hyetographs and topographic data to enable fast predictions of flood depths for other
125 rainfall events and locations (out of training sample data) complemented by 2D hydrodynamic
126 simulations. Guo et al. (2021) used a convolutional neural network (CNN) model trained on flood
127 simulation patch data from the CADDIES cellular-automata model to perform image-to-image
128 translation for rapid urban flood prediction and risk assessment. To simulate maximum flood
129 extent and depth, Hosseiny et al. (2020) created a system that combines a hydraulic model with
130 ML algorithms. Zahura et al. (2020) used simulations from high-resolution 1D/2D physically-
131 based models as training and test data for a random forest model that included topographic and
132 environmental characteristics to estimate hourly water depths. In these applications, flood depth,
133 which is important for risk assessments and damage estimates (Merz et al. 2010), has been

134 predicted by coupling physically-based and ML models. These coupled modeling studies
135 demonstrated the complimentary benefits of physically-based models along with ML algorithms
136 in producing flood modeling outputs, but the computational expense is still an application barrier.
137 Another significant challenge inherent in these studies lies in their dependence on hydraulic
138 models for training purposes. Furthermore, there is a gap in demonstrating the ability of these
139 studies to successfully predict flood characteristics beyond their training samples. For instance, no
140 studies have explored the capability of ML models to predict events other than those utilized in
141 their original training datasets (out-of-sample).

142 Despite previous efforts, the development of computationally efficient and user-friendly flood
143 prediction models remains a challenge. ML-based models, although promising and
144 computationally efficient, have not gained widespread acceptance among practitioners due to
145 concerns about their reliance on predicting flood characteristics for other events (out-of-sample).
146 Transferability is particularly crucial given the growing reliance on ML modeling methods, like
147 ANNs, as suggested by Wenger and Olden (2012). The term “transferability” refers to the model's
148 ability to predict different flood events beyond the scope of its training data, validating its
149 applicability to unseen scenarios, potentially with their unique characteristics (Jiang et al. 2024;
150 Wagenaar et al. 2018). Furthermore, there has yet to be research investigating the extent to which
151 flood depths prediction models can be transferred and applied successfully to different events
152 beyond the initial training settings. It, therefore, remains unclear whether an ML-based model,
153 which is trained, validated, and tested against a historical event, performs satisfactorily in
154 predicting flood characteristics of other events in the same watershed. Floods originate from
155 various sources and the flood characteristics depend on the unique characteristics of storm events.
156 High wind events tend to generate storm surges that move upstream, while intense rainfall over

157 upstream watersheds leads to fluvial flooding that moves downstream towards the coast.
158 Conversely, slow-moving storm systems can cause intense local rainfall, resulting in overland
159 runoff entering rivers along their paths rather than a concentrated upstream inflow flood wave.
160 Hence, it is crucial to avoid overfitting an ML model to a single historical flood event, as it can
161 lead to significant underperformance in handling other events.

162 A further limitation of past research is the sole focus on predicting greatest flood extents using
163 classification-based algorithms, while the performance of regression-based ML models for
164 predicting other important characteristics like flood depths has not been investigated. Additionally,
165 the importance of spatial distribution of input features has been overlooked in past ML-based flood
166 modeling. To hindcast a flood characteristic at a given location, the features have been
167 incorporated at that location, but flooding is generated through contributions by several other
168 factors that are relevant across the upstream contributing watershed (in inland systems) and/or
169 from the downstream coastline (in coastal systems).

170 This paper aimed to fill the abovementioned research gaps by examining the performance and
171 transferability of ML models in hindcasting maximum water depths across various events in a
172 coastal watershed. Our objective was to develop a transferable, computationally efficient model to
173 hindcast maximum water depths. We aim to evaluate the performance of ML models, which are
174 trained and tested based on an event, and shed insights on the application of the model for
175 predicting maximum river flood depths for other events as well. Our study developed a modeling
176 framework based on an ML algorithm, Multi-Layer Perceptron (MLP) architecture for our ANN
177 model. This algorithm was coupled with feature selection methods and geospatial data. We
178 evaluated the performance of this model against one extreme flood event, Hurricane Ida, across a
179 coastal watershed (six-digit hydrologic unity code [HUC6])—Lower Hudson—in Northeastern

180 US. Next, we assessed the transferability of our developed model across three other extreme
181 events—Hurricanes Isaias, Sandy, and Irene—in the same watershed. These events encompass
182 varied rainfall intensities, wind speeds and storm track directions. Unlike past ML-based modeling
183 studies, which focused solely on predicting flood status (flooded or unflooded), our regression-
184 based model estimates maximum water depths. This model was also examined against multiple
185 events, more than one single event that has been the focus of past research. The model also
186 considered the spatial dimension for predicting maximum water depths at a given location, in
187 which the features were represented either at that location or across the contributing watershed.
188 This ML model is generic and can be applied to hindcast maximum water depths at non-gauge
189 river sites to get a denser reconstruction of an event along the river network and hindcast water
190 depths in watersheds with similar drainage area (HUC6 or larger) and flood type (fluvial and
191 coastal).

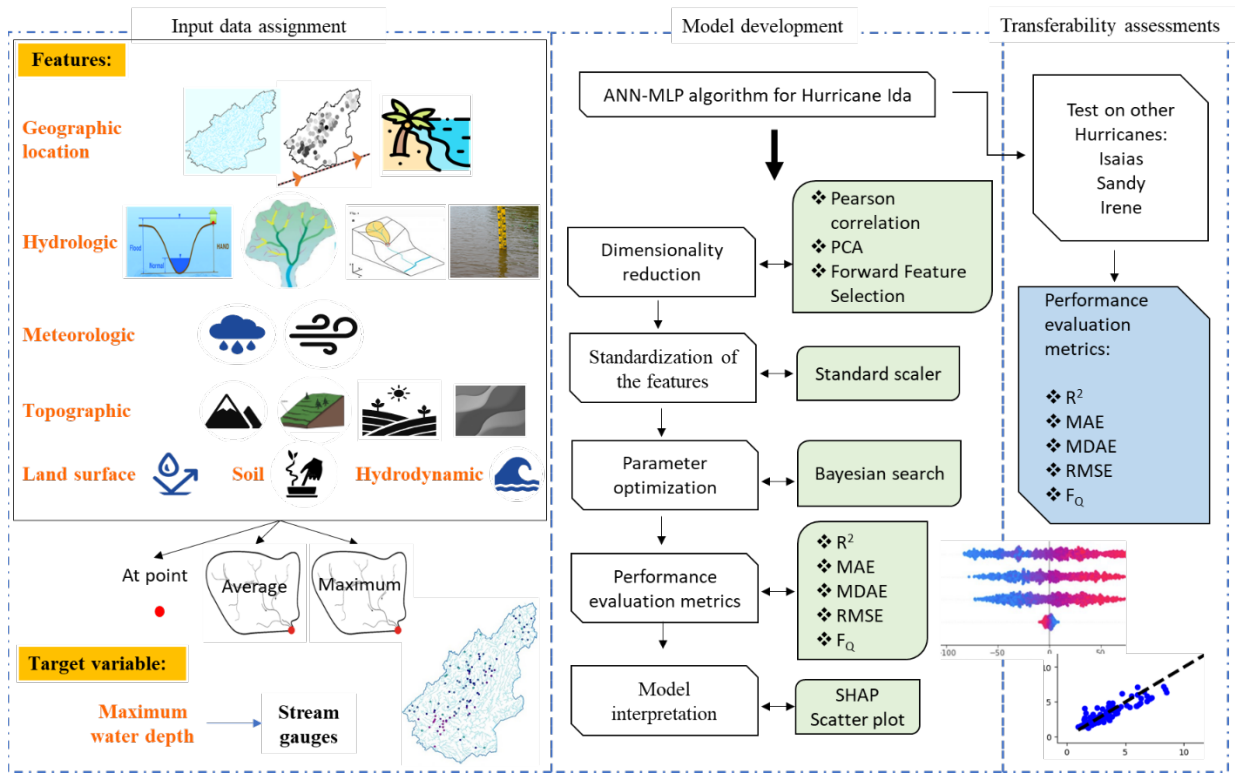
192

193 **2. Methodology**

194 We developed an ML-based model that hindcasts maximum water depths at stream gauges
195 across a coastal watershed during a flood event (Figure 1). A coastal watershed receives flood
196 contributions from the inland and coastal systems (e.g., fluvial and tidal). The model uses
197 geospatial analyses and ML algorithms to hindcast maximum water depths during an event at river
198 cross-sections of a given watershed. This model is informed by the underlying physical flood
199 processes represented by a wide array of features (topographic, meteorologic, hydrologic, land
200 surface, soil and hydrodynamic).

201 Geospatial operations were conducted to compute the features at stream gauges and/or over their
202 contributing watersheds (the upstream area that drains water to the gauge) considering the

203 underlying physical processes. We used feature selection techniques to determine the most key
 204 features for our ML model. Applying observed data from stream gauges during a flood event, the
 205 model was trained, cross-validated, and tested. We then evaluated the model transferability by
 206 examining its performance in three other extreme flood events.



207
 208 Figure 1. Schematic view of the machine learning (ML)-based model for hindcasting maximum
 209 water depths in coastal watersheds. PCA: Principal component analysis; SHAP: Shapley additive
 210 explanations; MAE: Mean absolute error; MDAE: Median absolute error; F_Q : Ratio of estimated
 211 over observed maximum flood depth.

212 **2.1. Selection and calculation of key features**

213 To develop a transferable ML model for complex physical phenomena of flooding, the
 214 selection process should extend beyond merely choosing features based on their individual
 215 statistical significance. Instead, it should focus on identifying features that collectively contribute

216 to a holistic representation of the phenomenon. We selected key features for our ML-based flood
217 model according to the past research and the underlying physical processes. Our model considers
218 these features from five broad categories of geographic location, hydrologic, topographic, land
219 surface, soil, and hydrodynamic (Table 1). Here, we provide information on how to derive the
220 features to hindcast maximum water depths during a flood event in a coastal watershed. Aside
221 from the soil category that represents pre-flood conditions (antecedent soil moisture), all other
222 features represent conditions during a flood event.

223

224

225 Table 1. Machine learning model features and the assignment approaches for stream gauges.

Category	Feature	Point-based	Spatial average across the contributing watershed	Spatial maximum across the contributing watershed
Geographic location	Distance to rivers		*	
	Distance from storm track	*		
	Distance from coastline	*		
Hydrologic	Height above nearest drainage (HAND)		*	
	Drainage area	*		
	Flow accumulation	*		
	Topographic wetness index (TWI)	*	*	
	Initial water depth	*		
Meteorologic	Rainfall depth	*	*	*
	Wind speed	*	*	*
Topographic	Elevation	*		
	Ground slope	*	*	
	Slope aspect	*	*	
	Slope aspect invariability (ASPVAR)		*	
	Curvature	*	*	
Land surface	Imperviousness		*	
Soil	Antecedent soil moisture	*	*	
Hydrodynamic	Storm surge	*	*	

226

227 By integrating all these factors into our methodology, we developed a flood hindcast model
228 that considers key processes in coastal watersheds. We used a two-step process to assign feature
229 values to a point located on a stream gauge. Depending on the feature, we assigned specified values
230 to the gauge itself or its contributing watershed to consider the spatial dimension in flood
231 generation processes. For the contributing watershed, spatial mean and maximum across the
232 contributing watershed of a given stream gauge was computed. This method ensures that the
233 feature values indicate the overall pertinent physical processes occurring at the streams and
234 upstream watersheds. Table 1 specifies how each feature was used in our model.

235 For features under the geographic location category, we incorporated distance to rivers—a
236 critical factor in determining flood risks (Cao et al. 2020; Rafiei-Sardooi et al. 2021), storm track—
237 specific to the flood event from (National Hurricane Center 2022)—and distance to the nearest
238 coastline. The proximity of a location to waterbodies, such as rivers or coastlines, directly
239 influences its vulnerability to flooding. Coastal regions are susceptible to storm surges, which
240 occur during tropical storms or hurricanes. Storm surges are massive walls of seawater that get
241 pushed ashore by intense winds. Storm tracks are pathways in the atmosphere along which storms
242 (e.g., hurricanes, tropical cyclones, or extratropical storms) tend to move. These storms often carry
243 heavy rainfall, intense winds, and storm surges, which can lead to severe flooding in areas they
244 pass over or affect. The distance to storm track and coastline is both considered “Point-based” as
245 they are specific to individual locations. However, distance to rivers is identical (zero) at these
246 stream gauges, but different in the contributing watersheds; we calculated the spatial average
247 distance of the contributing watersheds to the rivers.

248 Under the hydrologic category, we employed four variables of HAND, drainage area, flow
249 accumulation, topographic wetness index (TWI), and initial water depth. HAND represents the
250 elevation of a location relative to the nearest stream. This feature is widely used in flood modeling
251 due to its ability to hindcast flood-prone areas by considering topography and flow characteristics
252 (Hu and Demir 2021). As its value at the stream gauges is zero, its spatial average across the
253 contributing watershed was considered. The drainage area provides information about potential
254 runoff, while flow accumulation feature helps predict flow paths during flood events that is
255 previously used by Löwe et al. (2021) and Pham et al. (2021). Both drainage area and flow
256 accumulation values at point of stream gauge (Point-based) were captured. TWI was used by

257 (Gudiyangada Nachappa et al. 2020; Löwe et al. 2021; Pham et al. 2021; Zahura et al. 2020; Zhao
258 et al. 2020) and calculated using Equation (1) (Beven and Kirkby, 1979).

$$259 \quad TWI = \ln\left(\frac{\alpha}{\tan(\beta)}\right) \quad (1)$$

260 where, α is the slope of the contributing watershed per unit contour length (as known as the specific
261 catchment area), and β is the local slope gradient in radians. The TWI value was considered both
262 point-based and spatial average across the contributing watershed to represent the specific location
263 and the overall characteristics of the contributing watershed. The last feature in this category was
264 initial water depth, which refers to the stream gauge height one day before the event; this feature
265 was considered point-based and explains initial conditions in the study rivers.

266 The meteorologic category features were precipitation (Rafiei-Sardooi et al. 2021) and wind
267 speed. Rainfall is the main driving force for floods (Mishra et al. 2022). Storms can bring intense
268 and prolonged precipitation to certain areas. If a storm passes over or near a location, it can result
269 in excessive precipitation, overwhelming local drainage systems and causing flooding in low-lying
270 or poorly drained areas. Wind speed is another feature that can influence the severity and extent
271 of flooding, especially during hurricanes. Intense winds during storms and hurricanes generate
272 large and powerful waves in the ocean. These waves can exacerbate the impact of storm surges,
273 causing even more coastal flooding as they crash onto the shore and flood areas even farther inland.
274 We obtained daily precipitation and wind speed data for the entire period of flood event from
275 weather stations of the National Oceanic and Atmospheric Administration National Centers for
276 Environmental Information (NOAA's NCEI 2022). Their maximum values over a flood event
277 were computed at each stream gauge. Using point-based precipitation and wind speed data, we
278 then created a spatially distributed rainfall and wind speed dataset by interpolating the maximum

279 values using the Inverse Distance Weighting (IDW) method (Hosseini et al. 2020). Rainfall depth
280 and wind speed are considered for point-based, spatial average across the contributing watershed,
281 and spatial maximum across the contributing watershed. These values capture the intensity of the
282 meteorologic conditions at individual points and the overall average and maximum values across
283 the upstream watershed.

284 Elevation, ground slope, slope aspect, aspect invariability (ASPVAR), and curvature were
285 features under the topographic category (Cao et al. 2020; Chen et al. 2023; Huang et al. 2022;
286 Khosravi et al. 2018; Rafiei-Sardooi et al. 2021; Sun et al. 2020; Fereshtehpour et al. 2024). DEM
287 with a resolution of 1/3 arc-second (~10 m) was acquired from the United States Geological Survey
288 (USGS 2022), National Elevation Dataset (NED). To remove any spurious depressions, the DEM
289 sinks were filled to account for artificial depressions that can impede the realistic simulation of
290 water flow, ensuring that the derived water pathways and other hydrologic computations reflect
291 true surface conditions (Khosravi et al. 2018; Zhu et al. 2013). Elevation, ground slope, slope
292 aspect, invariability of slope directions (ASPVAR), and curvature were all derived from the DEM.
293 Elevation allows us to identify low-lying regions prone to floods and hindcast the maximum water
294 depths. Ground slope is a key factor in driving water movement. The ground slope plays a crucial
295 role in determining the direction and velocity at which water flows across the landscape. On sloped
296 terrains, water flows along the path of least resistance. The slope angle determines the speed and
297 volume of surface runoff, influencing the potential for flooding. Slope aspect provides insights
298 into surface runoff distribution and flow accumulation by indicating the direction of the ground
299 slope that affects hydrologic processes (Gudiyangada Nachappa et al. 2020; Rafiei-Sardooi et al.
300 2021). Similar to Gudiyangada Nachappa et al. (2020), we divided the slope aspect into 10
301 categories: north (0° - 22.5° ; 337.5° - 360°), northeast (22.5° - 67.5°), east (67.5° - 112.5°), southeast

302 (112.5°-157.5°), south (157.5°-202.5°), southwest (202.5°-247.5°), west (247.5°-292.5°),
303 northwest (292.5°-337.5°), and flat (0°). ASPVAR values near zero indicate diverse watershed
304 slope aspects, while values approaching 1.0 imply a dominant direction (Wan Jaafar and Han,
305 2012). This feature provided information about surface runoff distribution and flow concentration
306 by specifying the direction that water would flow across the terrain (Dawson et al. 2006).
307 Additionally, analyzing the curvature helped us understand how it impacts flood events (Khosravi
308 et al. 2018; Pradhan 2009). Elevation was considered point-based, while ground slope and
309 curvature were considered both point-based and spatial average across the contributing watershed.
310 ASPVAR conceptually represents the spatial average across the contributing watershed.

311 The land surface category was represented by only one variable, imperviousness. The greater
312 the imperviousness, the larger the volume of surface runoff. Impervious surfaces increase both
313 volume and velocity of runoff due to their high surface smoothness and low friction to resist water
314 movement. This rapid flow of water can overwhelm natural waterways, increasing the risk of
315 flooding. We used the spatial average of imperviousness across the contributing watershed in our
316 model.

317 Soil category included antecedent soil moisture, which reflects the pre-storm saturation extent,
318 essential for runoff estimates and high moisture flux production from rain-bearing systems
319 (Jafarzadegan et al. 2023; Mishra et al. 2022; Karamouz et al. 2022; Ahmadisharaf et al. 2018).
320 Soil moisture was calculated one day before the storm and considered both point-based (local soil
321 moisture adjacent to the stream gauge) and spatial average across the contributing watershed. This
322 feature explains initial conditions in the study watershed.

323 In the hydrodynamic category, we used storm surge from tidal gauges on the coast NOAA
324 (2023). Storm surge was estimated as the difference between the maximum water depth and the

325 astronomical tide during a flood event. This feature is crucial in hindcasting coastal contributions
326 to flood events. If the flood event does not receive any coastal contributions, this category can be
327 removed from the list of model features. It is considered for both point-based and spatial average
328 across the contributing watershed.

329 2.1.1 Feature selection method

330 We employed multiple feature selection methods Pearson's correlation coefficients (Cao et al.,
331 2020; Chen et al., 2023; Lee et al., 2020) and PCA—a widely used technique in many ML
332 modeling studies (Abdrabo et al., 2023; Chang et al., 2022; Reckien, 2018)—and forward feature
333 selection that accounts for interactions among the model features. We applied a step-by-step
334 approach to utilize these three techniques.

335 First, the Pearson's correlation coefficients were used to assessing the linear relationships
336 among the features and target variable. The strength and direction of linear relationships were
337 evaluated using Pearson's correlation coefficients. These analyses enabled us to narrow down the
338 initial list of the features.

339 Next, PCA was applied to the features retained after the Pearson's correlation analysis. In the
340 PCA method, the contribution of each feature to the overall variance is quantified by examining
341 the eigenvalues associated with each principal component (Abdrabo et al. 2023). Compared to the
342 Pearson's linear correlation, the PCA can reveal underlying patterns or structures in the data that
343 are not immediately apparent. PCA allows us to understand how much variance each principal
344 component considers in the dataset, providing a clear measure of feature significance in terms of
345 explaining the data variance. By aggregating the absolute values across all features, we obtained
346 the importance for each feature, which enabled us to rank them in a descending order and omit
347 least important features.

348 Last, the forward selection method was applied on the features retained. This method then
349 incrementally added variables, weighing both their individual impact and interactions, enhancing
350 the model predictive performance by focusing on features with substantial influence on flood
351 depths (Macedo et al. 2019; Horel and Giesecke 2019; Macedo et al. 2019). This method adds
352 variables to a model based on their predictive power. This iterative process starts with no variables
353 and includes the most predictive one at each step, considering both its individual impact and its
354 interactions with already included variables. This selection continues until adding more features
355 does not significantly enhance the model performance metric in terms of Akaike Information
356 Criterion.

357

358 **2.2. Machine learning (ML) models**

359 2.2.1. Artificial neural networks (ANNs)

360 To hindcast flood depth, our target variable, we employed ANN with MLP architecture. This
361 algorithm was trained via observed maximum water depths from stream gauges using the key
362 features selected through our feature selection (Section 2.1). The choice of ANN was based on
363 previous successful applications in flood depth modeling (e.g., Dawson et al., 2006; Abrahart,
364 Kneale, and See 2004; Bafitlhile and Li 2019; Berkhahn, Fuchs, and Neuweiler 2019; Dawson et
365 al. 2006; Rumelhart, McClelland, and Group 1986; Zhu, Yang, and Ren 2023). One of the
366 strengths of using ANNs in modeling tasks like flood predictions is their notable flexibility and
367 capability to approximate complex, non-linear relationships, potentially enhancing their
368 performance for unseen data. It is essential, however, to acknowledge that the capacity to
369 generalize depends on selecting relevant features that explain the underlying physical processes
370 and the spatiotemporal variability, model selection, parameterization, and training the model.

371 ANNs are designed to simulate the behavior of biological systems composed of "neurons". These
372 algorithms composed of nodes, or "artificial neurons", connected and operate in parallel. Each
373 connection is assigned a weight that represents its relative importance. During the learning phase,
374 the network learns by adjusting these weights based on the input data it is processing (McCulloch
375 and Pitts, 1943). Here, ANN was implemented using python's Keras library with TensorFlow
376 backend.

377

378 2.2.2. Machine learning (ML) model pre-processing and implementation

379 The observed water depths and features were split into training and testing sets, with 70% to
380 90% of the data used for training and 10% to 30% for testing as suggested by Joseph (2022) and
381 Nguyen et al. (2021). After exploring various splits within the 70% to 90% range for training data,
382 the 90% allocation for training (104 out of 116 stream gauges) was determined to be optimal for
383 our specific dataset and model based on preliminary testing, the model complexity, and the desire
384 to maximize the amount of data used for training while still retaining satisfactory results for the
385 test phase (12 out of 116 stream gauges). While the train percent (90%) seems high and suggests
386 potential for model overfitting, this same model was most successful in the transferability across
387 other three flood events (out-of-sample). The allocation of 10% of the data for testing serves to
388 provide an unbiased appraisal of the model generalization performance after training and
389 hyperparameter optimization. This evaluation process, complemented by methodologies such as
390 cross-validation and hyperparameter optimization, is structured to identify a model configuration
391 that is likely to perform well across unseen data. This approach aims to ensure that the final model,
392 selected based on its performance on the validation set during hyperparameter optimization, is
393 tested on entirely unseen data to confirm its generalization ability. In preparing our dataset for the

394 neural network model, numerical features were standardized to have a mean value of zero and a
395 standard deviation of one. This scaling process ensured that each feature contributes
396 proportionately to the model predictions, mitigating the potential bias towards variables with larger
397 scales.

398 Hyperparameter optimization is a step in improving the performance of ML models. This
399 process involves identifying the optimal hyper-parameter values. We used Bayesian Search to
400 perform hyperparameter optimization. Cross-validation, particularly through methodologies like
401 the Prediction Sum of Squares criterion for predictor selection and for parameter estimation and
402 predictive error assessment, has been foundational in improving predictive models. This approach
403 distinguishes between model selection and assessment (Allen 1974; Geisser 1975; Stone 1974).
404 Cross-validation was performed using a 5-fold cross-validation strategy during the hyperparameter
405 optimization process. Opting for 5-fold cross-validation over hold-out validation in our
406 hyperparameter optimization process reflects a balance between comprehensive model evaluation
407 and computational efficiency. The hyperparameters we optimized here included the number of
408 layers, units, activation functions, optimizer, regularization rate, batch size, and epochs. Bayesian
409 search offered a targeted search based on probabilistic modeling, iteratively refining the search
410 area based on past evaluations to efficiently select the most promising hyperparameter sets. The
411 selection of the optimal hyperparameters was guided by minimizing the cross-validation MSE,
412 ensuring the chosen configuration significantly improved the model predictive performance for
413 maximum water depths. The ANN-MLP model was trained using the training data and the best
414 hyperparameters obtained from the optimization process.

415 To prevent overfitting, we used early stopping and model checkpointing during the model
416 training. Early stopping was implemented to stop training when the validation loss stopped

417 improving, and model checkpointing was used to save the model with the lowest validation loss.
418 The strategy involved splitting the training data into five subsets and training the model five times,
419 each time using a different subset as the validation set. This evaluation process, complemented by
420 methodologies such as cross-validation and hyperparameter optimization, is structured to identify
421 a model configuration that is most likely to perform well across unseen data.

422 2.2.3. Model performance evaluation

423 The performance of the ANN-MLP model was evaluated using coefficient of determination (R^2),
424 mean absolute error (MAE), normalized root mean square error (NRMSE), median absolute error
425 (MDAE), and the ratio of estimated over the observed maximum flood depth (F_Q ; Schubert and
426 Sanders 2012). The R^2 metric measures the proportion of variance in the dependent variable
427 predictable from the independent variables. The MAE measures the average magnitude of the
428 errors in a set of estimations without considering their direction (i.e., overestimation or
429 underestimation). The NRMSE is a metric that quantifies the normalized average magnitude of the
430 prediction error. It assesses the relative size of the root mean square error (RMSE) by considering
431 the RMSE in relation to the average value of the observations. It is commonly used in regression
432 analyses and a smaller NRMSE value indicates a higher level of agreement between the estimated
433 values and the actual observations (Stow et al. 2003; Ahmadisharaf Ebrahim et al. 2019). The
434 MDAE is a metric that measures the median of the absolute differences between predicted values
435 and actual (observed) values. Unlike the MAE, which averages these differences out, the MDAE
436 focuses on the midpoint of these differences, making it less sensitive to the outliers. This
437 characteristic can make the median error a more robust metric in the regional water depth
438 estimation where the data contains significant outliers. It is a common metric used in ML models

439 such as Sheridan et al. (2019); Dixit et al. (2022); Park, Ju, and Kim (2020). These metrics were
440 calculated for both training and testing datasets to assess the model performance.

441 2.2.4. Model explainability

442 To interpret the model and explore the contribution of each feature to the estimation, we used
443 SHAP that is a game theoretic approach to explain the output of an ML model (Lundberg and Lee,
444 2017). It connects optimal credit allocation with local explanations using the classic Shapley
445 values from game theory and their related extensions. The SHAP values interpret the impact of
446 having a certain value for a given feature in comparison with the estimations we would make if
447 that feature took some baseline value (Abdollahi and Pradhan, 2021). In other words, SHAP
448 estimates how much each feature contributes to the model prediction output for a particular
449 instance. The SHAP results on the feature importance and their impacts on the model prediction
450 can be presented using a plot to visually show the distribution of impacts of each feature on the
451 model output. A positive SHAP value indicates that the feature's presence increases the model
452 output, while a negative SHAP value indicates that it decreases the model output. Further, we
453 visually evaluated the performance of our model in terms of bias (overestimation and
454 underestimation) using scatter plots.

455

456 **2.3. Model transferability across flood events**

457 The ML-based model, which was initially developed, trained, and validated based on one flood
458 event, was subsequently examined as is (with no additional parameter tuning) against other events
459 in terms of the performance and generalizability in hindcasting maximum water depths. By
460 examining our model against different flood events, we aimed to evaluate its effectiveness in
461 hindcasting maximum water depths across diverse events. This evaluation allowed us to assess the

462 ML model ability to handle varying flood conditions and its potential for application in different
463 events in the same watershed.

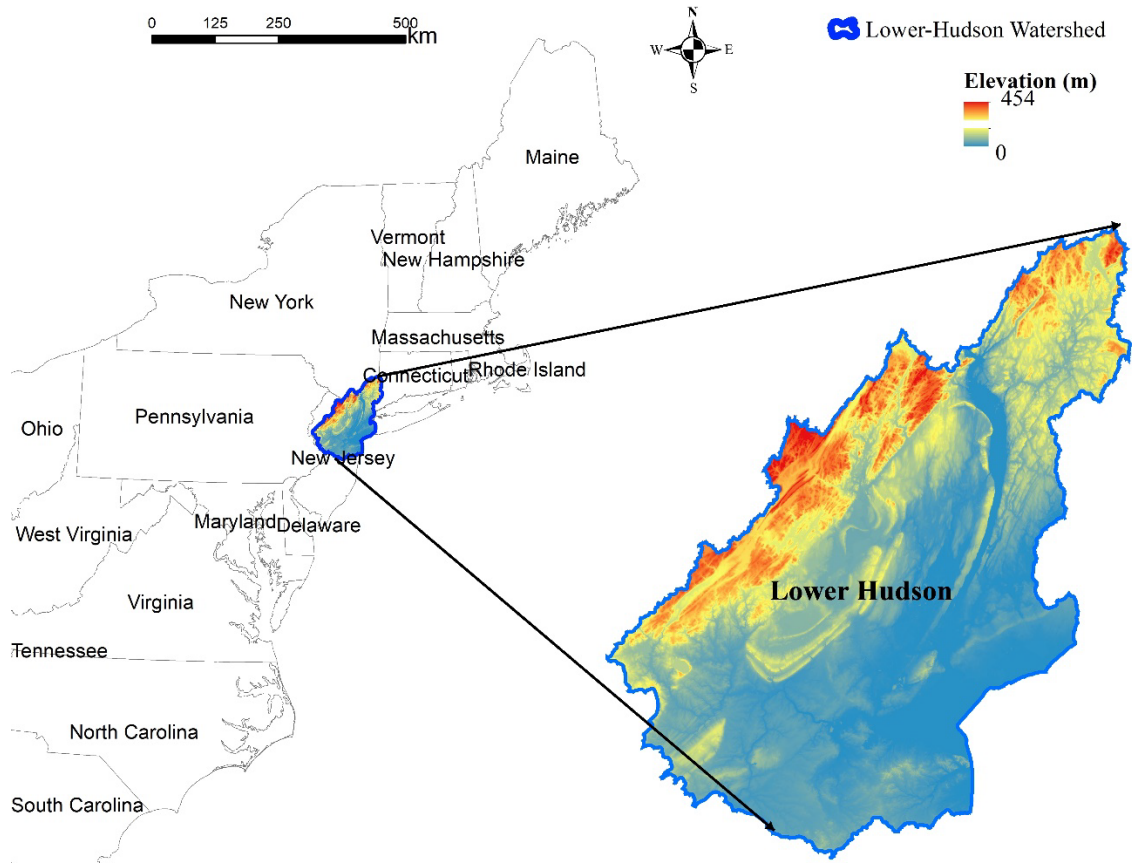
464

465 **3. Study area**

466 The study area is a HUC6 watershed, the Lower Hudson Watershed (HUC 020301). The
467 10,068 km² watershed is in the Northeastern United States (Figure 2) spanning parts of three states,
468 Connecticut, New Jersey, and New York. This watershed has a humid subtropical climate with hot
469 summers and mild winters. The highest elevation is ~450 m above mean sea level. Residential,
470 agriculture, and forest are the dominant land uses in the watershed according to the 2021 National
471 Land Cover Dataset (NLCD) (USGS 2022). Large metropolitan areas like New York are in the
472 study watershed. Several major rivers drain into the watershed, including the Hudson River, which
473 flows for 496 km (about the length of New York State). The ground slope varies from 87.5% in
474 the mountainous parts to near zero in the coastal parts.

475 We studied four major flood events in the study area. The primary event for model
476 development was Hurricane Ida in 2021, while three other hurricanes—Isaias (2020), Sandy
477 (2012) and Irene (2011)—were used to assess the model transferability. Hurricane Ida, a
478 devastating Atlantic Category 4 hurricane that made landfall in September 2021, hit Louisiana,
479 and progressed toward the Northeastern United States. The hurricane caused considerable floods
480 and significantly impacted both the west-south-central region, including New Orleans, and the
481 northeastern region, with severe damages reported in New York City and Philadelphia (Beven II,
482 Hagen, and Berg 2022; Wang et al. 2022). The storm remnants sent record-breaking rainfall to the
483 New York region as they headed northeast, resulting in flash flooding (Beven II, Hagen, and Berg
484 2022). The extensive flooding and severe property destruction caused by Hurricane Ida's record-

485 breaking rains highlighted the importance of comprehending the hurricane effects on affected
486 areas. Furthermore, strengthening regional resilience to catastrophic flooding episodes requires the
487 development of effective mitigation strategies. The three other events, which were used to evaluate
488 the model transferability, were also most recent major hurricanes after 2000, with available
489 streamflow data and differing track and intensity. In 2020, Hurricane Isaias, a Category 1
490 hurricane, made a quick trip along the East Coast, bringing with it severe rain and floods, especially
491 in the Mid-Atlantic and Northeast. The storm's rapid passage caused several deaths and extensive
492 power losses (Latto, Hagen, and Berg 2021). In 2012, superstorm Sandy, commonly known as
493 Hurricane Sandy, struck the Northeast and caused severe damage. It produced significant flooding
494 due to the intense storm surge and torrential rains, especially in New York and New Jersey, where
495 the storm surge reached record heights (Blake et al. 2013). In 2011, a huge and catastrophic storm
496 named Hurricane Irene affected a major portion of the Eastern Seaboard. Heavy rains from the
497 storm caused significant flooding, especially in Vermont, where it was the worst flooding in over
498 a century for that state (Lixion and Cangialosi 2013).



499

500

Figure 2. Lower Hudson River Watershed.

501 **3.1. Data collection**

502 Table 2 lists the data used for the study area alongside their source and spatiotemporal
 503 resolutions. We acquired instantaneous stream gauge height data from the USGS’s National Water
 504 Information System to analyze water depths during the four flood events. While the features’ data
 505 had different spatial resolutions, we did not make them consistent because only at-point (stream
 506 gauges) or aggregated spatial statistics of contributing watersheds were used in the ML model; no
 507 combinations of the features were needed.

508 Table 2. Model features and data sources and resolutions in the study area. NHDPlus: National
 509 Hydrography Dataset Plus; NED: National Elevation Dataset; NWIS: National Water
 510 Information System.

Category	Feature	Source	Spatial resolution	Temporal resolution
Geographic location	Distance to rivers		—	—
	Distance from storm track	NHDPlus	—	—
	Distance from the coastline		—	—
Hydrologic	Height above nearest drainage (HAND)	NED	10 m	—
	Drainage area		—	—
	Flow accumulation		—	—
	Topographic wetness index (TWI)		—	—
Meteorologic	Initial water depth	NWIS		
	Rainfall depth	NCEI	—	Daily
	Wind speed			
Topographic	Elevation			—
	Ground slope	NLCD	10 m	—
	Invariability of slope directions (ASPVAR)			—
	Curvature			—
Land surface	Imperviousness	NLCD	30 m	—
Soil	Antecedent soil moisture	ERA5	—	Daily
Hydrodynamic	Storm surge	NOAA Tides and Currents	—	Sub-hourly

511

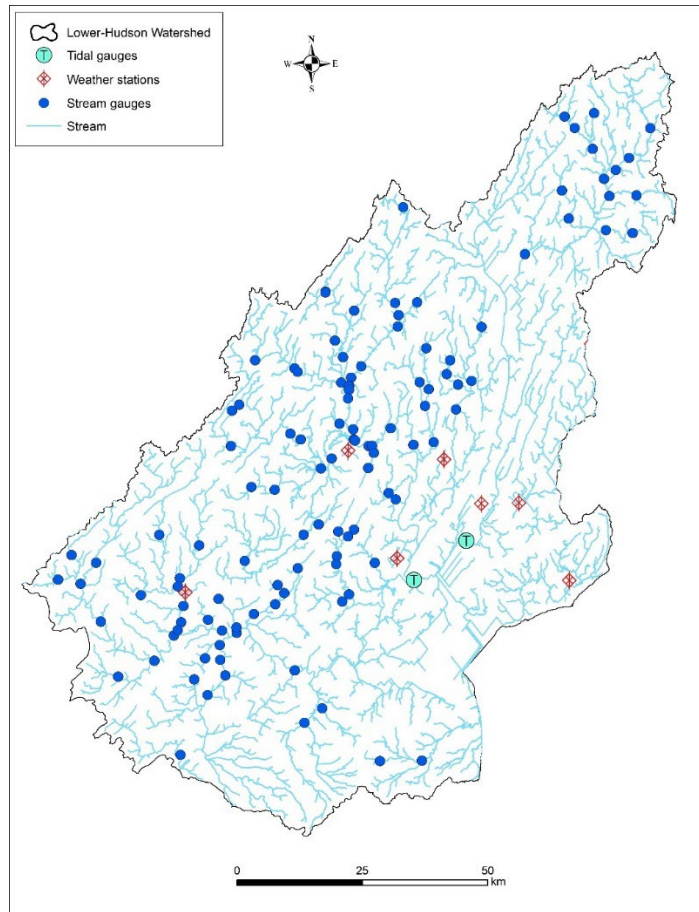
512 The study watershed embraces 116 stream gauges, seven weather stations and two tidal gauges
 513 (Figure 3). These gauges and stations recorded data for all the four events (Hurricanes Ida, Isaias,
 514 Sandy, and Irene). The drainage area of the contributing watersheds of the stream gauges varies
 515 from 5.5 to 2,104 km². The range of maximum recorded maximum water depths, rainfall, and
 516 antecedent soil moisture near the stream gauges during the four hurricanes are presented in Table
 517 3. It shows that Hurricanes Ida and Irene associated with much higher rainfall depths. These
 518 increased precipitation levels contribute directly to flood severity, as they can overwhelm drainage
 519 systems and lead to runoff exceeding riverbank capacities. The percent soil moisture before the

520 storms ranged from fairly dry conditions (9%) to nearly half saturated (43%). Ida and Irene had
 521 similar antecedent soil moisture conditions, which influenced their respective river water depths.
 522 Hurricane Sandy had a higher antecedent soil moisture percentage range of 17% to 38% compared
 523 to both Ida and Isaias, indicating a potentially higher level of saturation before the storm arrival.
 524 This likely contributed to Sandy's significant storm surge, which ranged from 1.97 to 2.85 m,
 525 compared to Ida and Isaias with storm surge ranges of 0.25 to 0.67 m and 0.20 to 0.76 m,
 526 respectively. Maximum wind speeds during these events were quite high, especially for Hurricanes
 527 Isaias, Sandy, and Irene. The proximity to the central path of the storm influences the intensity of
 528 the rainfall, wind speed, and storm surge experienced. Shorter distances to the storm track,
 529 particularly in Ida and Irene, correlated with more severe weather conditions and, consequently,
 530 greater flood depths.

531 Table 3. The range of river water depth, cumulative rainfall depth and antecedent soil moisture in
 532 the flood events.

Event	Year	River water depth (m)	Cumulative rainfall depth (mm)	Antecedent soil moisture (%)	Storm Surge (m)	Wind speed (m/s)	Distance to storm track (m)
Ida	2021	0.85-36.66	121.92-201.81	21-43%	0.25-0.67	27.64-35.49	0.09-1.1
Isaias	2020	0.22-35.35	17.37-62.22	9-39%	0.20-0.76	48.29-65.33	0.23-1.14
Sandy	2012	0.24-35.98	19.83-56.53	17-38%	1.97-2.85	63.43-76.97	0.77-2.16
Irene	2011	1.03-37.33	147.29-217.74	19-43%	1.05-1.37	51.05-60.68	0.00-0.93

533



534

535

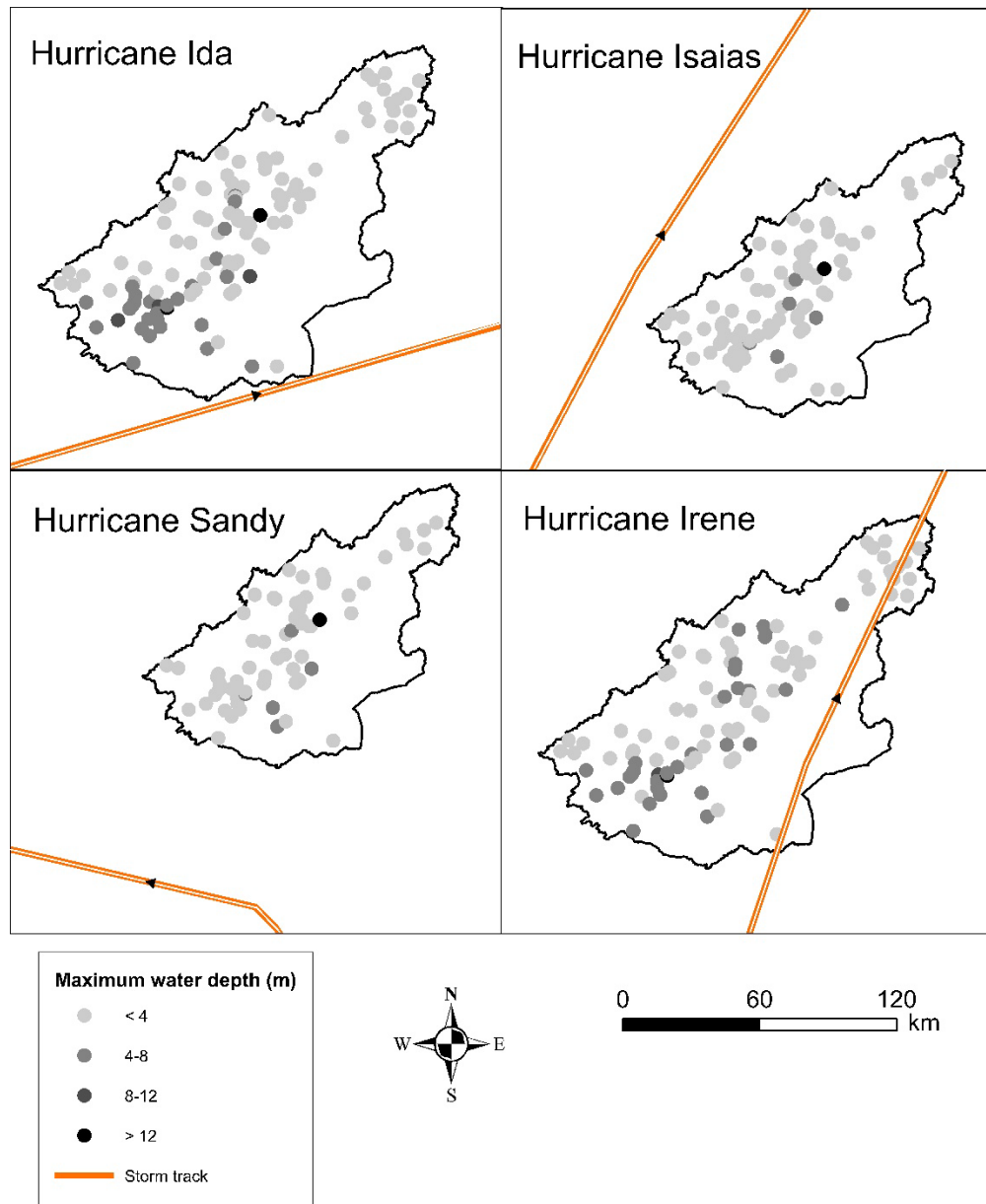
Figure 3. Stream and tidal gauges and weather stations in the study watershed.

536

537

Figure 4 displays the spatial variability in maximum water depths and storm tracks for all hurricanes. The total slope aspect was south, which resulted in shallower depths at the river upstream. As we moved southward along the river mainstream, water depths became deeper.

538



539

540 Figure 4. Maximum water depths across the study area during the four study hurricanes.

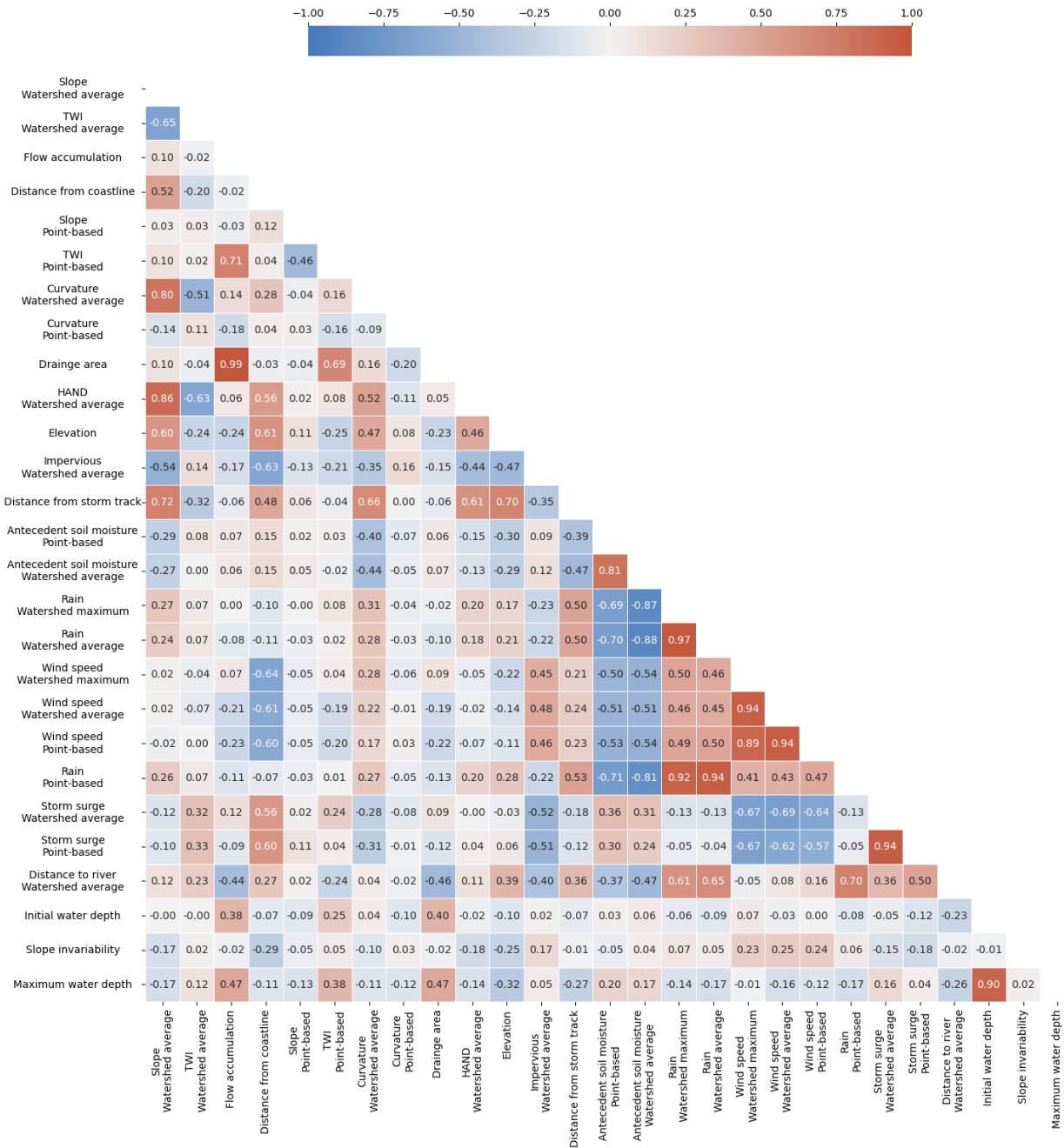
541

542 4. Results and discussion

543 4.1. Feature selection

544 Using Pearson's correlation analyses, we eliminated five features with absolute correlation
 545 coefficients >0.70 , the cutoff threshold suggested in previous studies (Cao et al. 2020; Chen et al.

546 2023; Lee et al. 2020). According to Figure 5, the strong correlation coefficient of 0.99 between
547 drainage area and flow accumulation, indicated that both features capture similar information
548 about water flow and storage in the watershed. To avoid collinearity issues, flow accumulation
549 was excluded from further analyses due to its weaker correlation with flood depth. Similarly,
550 features that demonstrated weaker correlations with flood depth or were highly correlated with
551 multiple features, were excluded. These analyses ensured that independent variables, which are
552 essential for modeling maximum water depths, are retained in our modeling.



553

554 Figure 5. Heatmap of Pearson correlation matrix for the initial model features.

555 Next, we conducted PCA to assess the importance of the features retained by Pearson's
 556 correlation analyses in hindcasting maximum water depths. The analyses showed that the slope at
 557 the stream gauge, slope aspect, slope invariability, curvature at the stream gauge, and average

558 curvature across the contributing watershed were the least important features for capturing the
559 overall variability of maximum flood depth. Consequently, we excluded these features from our
560 analyses. The lesser importance of slope at the stream gauge and slope aspect may be since river
561 slope is related to bathymetry, which is typically not represented well by DEMs (Bhuyian and
562 Kalyanapu 2020).

563 The forward feature selection method showed that initial water depth, elevation, TWI,
564 antecedent soil moisture, rainfall, and distance from storm surge at the stream gauge (all point-
565 based), as well as average storm surge and maximum wind speed across the contributing
566 watershed, along with their interactions were selected for the final ML model. Considering the
567 interactions among the features improved the model performance. This was expected because a
568 combination of some of the features better explain the underlying physical processes. For instance,
569 using the combination of storm surge and TWI as one unified feature can be an indication of the
570 physical propagation of storm surge that occur primarily in waterways.

571

572 **4.2. Machine learning (ML) model development**

573 4.2.1. Model development and performance evaluation

574 In the development of our ANN-MLP model for hindcasting maximum water depths during
575 Hurricane Ida, we used Bayesian search with a cross-validation strategy for hyperparameter
576 optimization. Details of the optimization can be found in Supplementary Material.

577 The model demonstrated an excellent performance on the training dataset ($R^2 = 0.94$, MAE =
578 0.64 m, MDAE = 0.44 m, and NRMSE = 24%). On the test dataset, the model achieved an R^2 of
579 0.91, the MAE of 0.77 m, MDAE was 0.42 m, and the NRMSE was 28%, further suggesting the
580 satisfactory performance by the model. The training history plot showed that the model

581 performance improved with each epoch during training, indicating that the model was learning
582 from the data. The model training process stopped at epoch 87 due to early stopping.

583

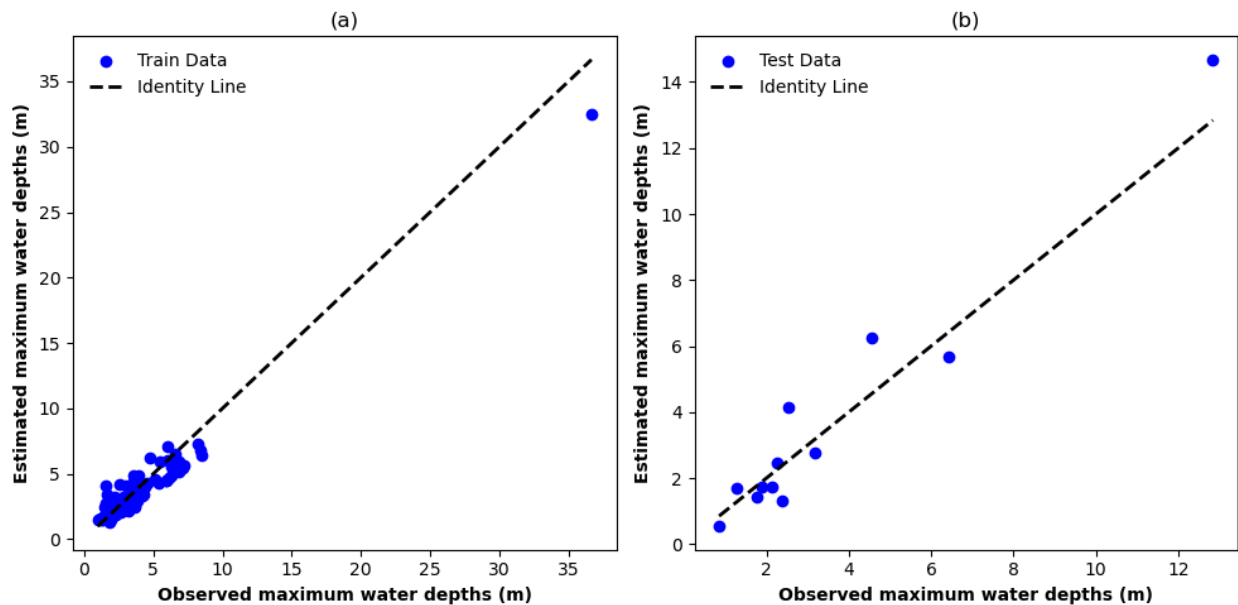
584 4.2.2. Model explainability

585 Figure 6 shows the performance of the ML model in hindcasting maximum water depths at stream
586 gauges, comparing estimated values against observed values for both training and testing datasets.

587 In the training phase (Figure 6a), points are clustered along the identity line, but tend to
588 underestimate large water depths. This pattern suggested that the model learned the training data

589 well, especially for smaller water depths, but did not fully capture the behavior that leads to the
590 larger water depths. The underestimation of high values is expected due to the lower number of

591 observations. The test data (Figure 6b) revealed a similar pattern of underestimation towards
592 higher values; this can be since the number of observed high water depths is small.

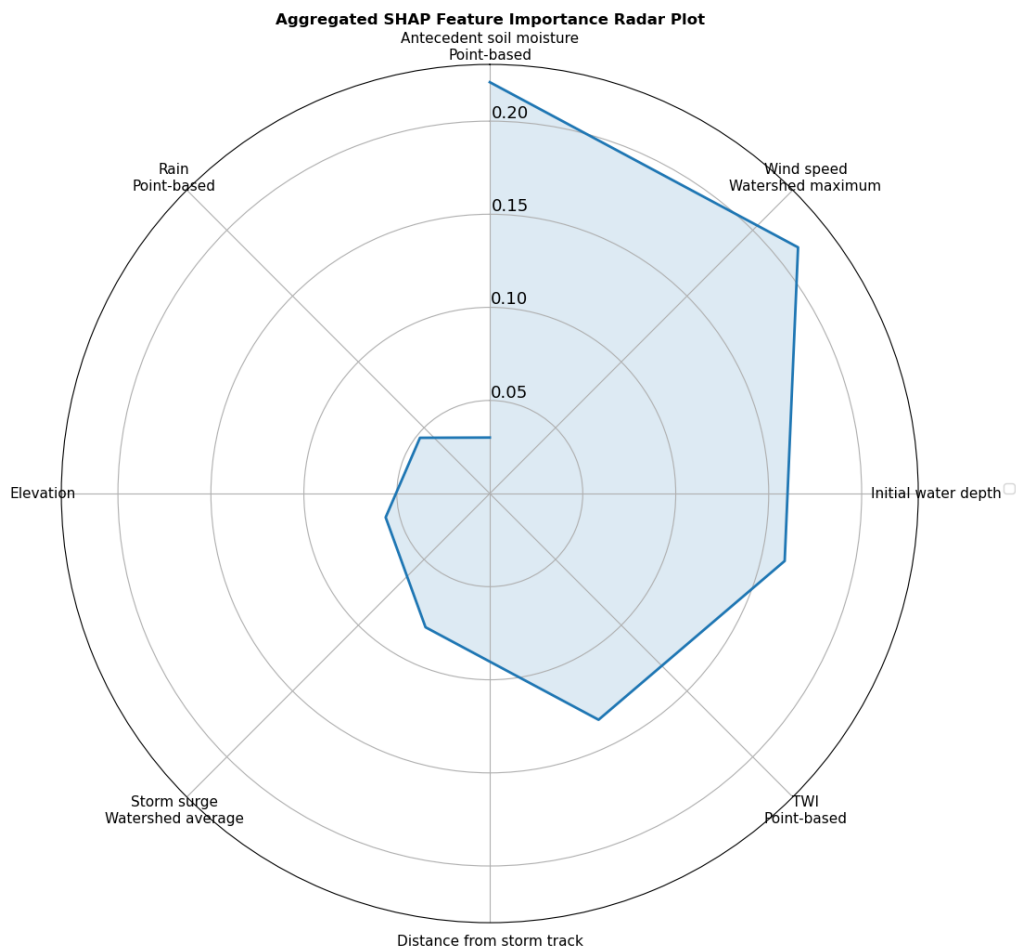


593

594 Figure 6. Scatter plots of estimated vs observed maximum water depths for: (a) train and (b) test

595 data. The identity line represents a perfect match between the estimated and observed values.

596 Figure 7 provides an overview of the influence of distinctive features on the model estimation
 597 on maximum water depths. Features like the antecedent soil moisture and maximum wind speed
 598 across the contributing watershed were found to substantially influence the water depth
 599 estimations. The inclusion of elevation as an important feature in our study closely aligns with the
 600 findings of Hosseini et al. (2020) and Chen et al. (2023) in their flash flood susceptibility and
 601 hazard assessments on a small non-tidal and a large coastal watershed. Elevation has been
 602 recognized as a crucial factor influencing flood occurrences, as it directly affects the water flow
 603 and drainage patterns within a watershed (Rafiei-Sardooi et al. 2021).



604 Figure 7. Aggregated Shapely additive explanations (SHAP) feature importance radar plot of the
 605 ML model for hindcasting maximum water depths.
 606

607 On the other hand, features such as the interaction of initial water depth and rainfall and local
 608 rainfall were identified as the least key features in estimating maximum water depths. In a coastal
 609 context, where the landscape reaction to oceanic events often overshadows rainfall affect, this
 610 outcome is noticeable. The finding about the less importance of rainfall in flood estimation concurs
 611 with the results by Salvati et al. (2023) in pinpointing vulnerable regions within a non-coastal
 612 medium-sized watershed. The study suggested that rainfall may have a lower impact on flood
 613 occurrences or flood depth estimations compared to other influential factors. The consideration of
 614 the interactions between rainfall and other features may also obscure the direct influence of rainfall
 615 on the model's predictions, especially in complex flood modeling.

616 It is important to note that the least important features are not necessarily uninformative; they
 617 simply contribute less to the model's output relative to the most important features. This can be
 618 due to the nature of the data, the modeling approach, or the specific context of the problem being
 619 addressed.

620 **4.3. Examining the machine learning (ML) model transferability across flood events**

621 The transferability of the trained and tested model (against Hurricane Ida) was examined by
 622 applying it to three other events within the same watershed. Table 4 summarizes the evaluation
 623 metrics for the three hurricanes.

624
 625 Table 2. Model performance across in historical flood events. MAE: mean absolute error;
 626 MDAE: Median Absolute Error; RMSE: root mean square error; F_Q: ratio of estimated over
 627 observed maximum flood depth.

Flood event	R ²	MAE (meters)	MDAE (meters)	NRMSE (%)	F _Q (%)
-------------	----------------	-----------------	------------------	--------------	-----------------------

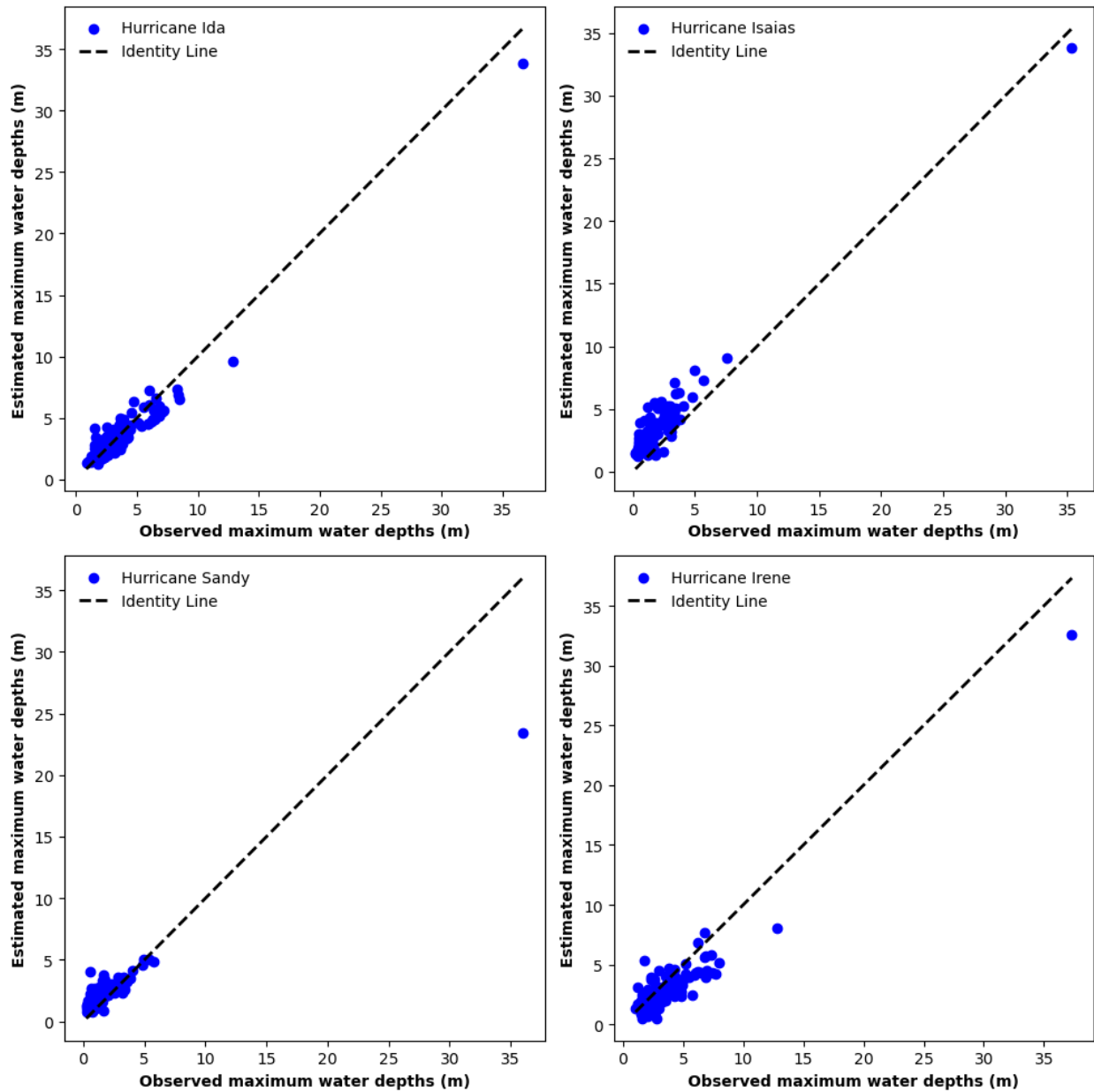
Original model					
Hurricane Ida	0.94	0.64	0.45	24.1	138.1
Transferability					
Hurricane Isaias	0.73	1.54	0.85	86.3	325.6
Hurricane Sandy	0.70	1.71	1.78	109.2	370.2
Hurricane Irene	0.85	1.12	0.85	36.7	112.6

628

629 These results demonstrated the model ability to transfer across different hurricanes within the
630 same watershed ($R^2 > 0.70$). With an MAE less than 1.71 m in all hurricanes, our model
631 performance is consistent with the CNN model of Guo et al. (2021), demonstrating its capability
632 for satisfactory flood depth estimates. However, when compared to the original model
633 performance on Hurricane Ida, the R^2 values and other metrics show weaker model performance
634 for the transferability to other hurricanes, suggesting reduced estimative accuracy, but not to the
635 extent that the model performance becomes unsatisfactory.

636 Figure 8 shows the relationship between observed and estimated maximum water depths for
637 the four storm events. Most observed water depths for the hurricanes were low. For all four events,
638 the data points suggested that the model tends to underestimate the high water depths and
639 overestimate the low water depths (Figure 8). The plots for Hurricanes Sandy and Irene show a
640 more dispersed set of points, suggesting a wider variance in the model estimates compared to the

641 observations. This implied that the model is less accurate in capturing the flood dynamics of these
642 events or that these events have unique characteristics that are not fully learned by the ML model.



643
644 Figure 8. Scatter plots of estimated vs observed flood depth for the four hurricanes.

645 For Hurricane Ida, our original model, 32% of the stream gauges had an F_Q between 90% to
646 110%, implying satisfactory estimates at these gauges (Gallegos, Schubert, and Sanders 2012;

647 Schubert and Sanders 2012). Hurricanes Irene, Sandy and Isaias had fewer gauges with moderate
648 F_Q values of 16%, 14% and 3.5% out of all stream gauges respectively, suggesting that the model
649 estimations were less satisfactory for these events compared to Ida in terms of bias. However, the
650 transferability was still more successful for Irene than the other two hurricanes, similar to what we
651 found based on the other metrics (Table 4).

652 We attributed the model transferability performance to four main factors: water depth,
653 antecedent soil moisture, storm track and the primary driver of flooding. Based on Table 2,
654 Hurricanes Ida and Irene exhibited significant similarities in river water depths and antecedent soil
655 moisture, which influenced their respective river water depths. These two hurricanes had similar
656 antecedent soil moisture conditions, while Hurricane Sandy had a higher antecedent soil moisture
657 percentage range of 17% to 38% compared to both Ida and Isaias, indicating a potentially higher
658 level of saturation before the storm arrival. These partly explain the better model transferability
659 for Hurricane Irene compared to Hurricanes Isaias and Sandy is expected.

660 The original storm track of Hurricane Ida was located to the watershed southeast, moving
661 northeast, and remained fully outside the watershed (Figure 4). Hurricane Irene's path, which was
662 somewhat similar to Ida's, stretched from the southeast to the northeast, resulting in the best model
663 transferability. The key difference is that Irene's storm path lays inside the watershed along its
664 eastern border. Consequently, the model, assuming a track similar to Ida's (the event that the model
665 was trained for), underestimated maximum water depths during Hurricane Irene. For Hurricanes
666 Isaias and Sandy, which the storm track was farther from the watershed and dissimilar from Ida's
667 path, the model overestimated the water depths. Isaias' storm track moved from the southwest to
668 the northwest of the watershed, while Sandy's unique path propagated from the southeast to the
669 southwest, leading to the lowest satisfactory in terms of the model transferability among the events.

670 The other reason why the model transferability was most successful for Hurricane Irene was
671 that the event mainly driven by significant rainfall, similar to Hurricane Ida (the event that the
672 model was trained for). In contrast, the model performed worse for Hurricanes Sandy and Isaias
673 because these events were mainly driven by storm surge. The original model, considered lower
674 importance for storm surge, was not effective in predicting the water depths in Sandy and Isaias.
675 In fact, here we see another significant advantage of strategically using physically meaningful
676 features rather than the more commonly used black box approach. By considering the physical
677 phenomena in our model development, we can better understand its strengths and weaknesses and
678 more effectively evaluate its performance.

679 Despite these distinct characteristics of the storm events, the ML model demonstrated
680 satisfactory performance on Hurricanes Sandy and Isaias, suggesting some level of transferability,
681 mainly because we incorporated a wide array of pertinent flood influencing features and the spatial
682 dimension (contributing watershed). While the model performs well, the inconsistency of the
683 success level of transferability across flood events presents opportunities to incorporate additional
684 features or training approaches, enhancing the model robustness to different storm tracks relative
685 to the watershed and weighing the model features based on the main flood driver (e.g., rainfall or
686 storm surge).

687 The study underscored the complexity of efficiently predicting water depths for major
688 hurricanes and emphasizes the necessity of refining models for better performance during such
689 extreme events. It highlighted the importance of deeper analyses into features causing prediction
690 discrepancies and suggested that addressing different flood types (fluvial vs. storm surge)
691 separately can enhance the model performance. This approach, alongside adjustments for specific
692 flood characteristics like storm tracks and similar influential factors that are distinct for each event,

693 can improve the performance of hindcast models, aiding in the development of more transferable
694 ML-based models.

695

696 **4.4. Limitations and future research**

697 While this study showed promising results about ML-based flood modeling, it is important to
698 acknowledge its limitations to identify areas for future research. One limitation is the presence of
699 inherent uncertainties in the model that can impact the accuracy of the estimations. These
700 uncertainties can stem from various sources, including the quality and accuracy of the observed
701 data (Merwade et al. 2008; Bales and Wagner 2009; Gallegos, Schubert, and Sanders 2012; Teng
702 et al. 2017) and input data (features). For instance, relying solely on spatially aggregated values of
703 features (mean and maximum used in this study) may not adequately capture the spatial
704 heterogeneity of pertinent variables across the upper watershed. Future research should prioritize
705 addressing these uncertainties by exploring alternative data sources and methodologies. The ANN-
706 MLP model was tuned using observed flood data and an optimal hyperparameter set was used
707 based on the hyperparameter optimization methods. This deterministic approach does not
708 incorporate the uncertainty from model parameterization. Probabilistic models are needed to
709 address this uncertainty. Parameterization uncertainty acknowledges that the exact values of model
710 parameters (e.g., weights in an ANN-MLP) determined through training may not perfectly capture
711 the true underlying processes, leading to variability in our predictions. Probabilistic models
712 address this uncertainty by incorporating it directly into the modeling process, offering a range of
713 possible outcomes with associated probabilities (posterior probability distributions) rather than a
714 single deterministic output. This is achieved through techniques like Bayesian inference, where
715 prior knowledge about parameters is updated with observed data to produce a posterior distribution

716 of parameters. This approach provides a more nuanced understanding of uncertainty, allowing
717 predictions to reflect both the variability observed in the data and the confidence in the model's
718 parameter estimates. To address the limitations of deterministic models, like the ANN-MLP used
719 in this study, future research should explore integrating probabilistic modeling techniques such as
720 Bayesian inference. Exploring alternative data sources and methodologies, such as incorporating
721 spatially detailed features or dynamic time series data, could also help in capturing the
722 complexities of watershed characteristics more accurately.

723 Furthermore, we did not have sub-daily data available for all model features. Incorporating
724 sub-daily data can highly likely improve the model accuracy in capturing intra-daily variability
725 and flood dynamics, but it was not explored due to data constraints. Future research should
726 incorporate sub-daily data into flood depth hindcast models. A further limitation of this study
727 related to the time dimension is that wind events, storm surges, rainfall, and overland flow
728 processes have different time signatures. Pluvial and storm surge flooding can be closely
729 coincident with the storm event, but river flood waves may take much longer to arrive at a
730 particular location. The time lag between these processes was not considered in our ML model,
731 which was not dynamic in time and only hindcasted maximum river maximum water depths.
732 Incorporating time-variability of the features can better represent the time-varying nature of flood
733 dynamics.

734 Another limitation of this study is the issue of bathymetry that is typically not represented well
735 by DEMs like USGS' NED. Refining the DEMs with bathymetry data such as NOAA's
736 Continuously Updated DEM (CUDEM) dataset and channel cross-sections is recommended to
737 better represent the terrain on channels and floodplains in the model.

738 Additionally, we modeled maximum water depths across a large watershed (HUC6), whereby
739 many details may not be important. For small watersheds and specially urbanized ones, we
740 emphasize the importance of considering local factors such as sewer and drainage systems in flood
741 depth hindcast, where pluvial floods may be prevalent. However, obtaining data on sewer and
742 drainage systems can be challenging due to availability, lack of quality and confidentiality of the
743 data, particularly at the desired spatial and temporal resolutions. Future research should strive to
744 improve the availability and accessibility of such data to enhance the accuracy of flood depth
745 hindcasting, especially in urban areas. In small urban watersheds, other details such as land
746 management practices and other local features can also be important for flood depth hindcasting
747 and should be incorporated in the ML-based model.

748 This study primarily focused on hindcasting maximum water depths and did not consider other
749 important flood characteristics, such as duration, frequency, and extent, all of which are important
750 for loss estimates, decision making and risk management (Ahmadisharaf and Kalyanapu 2019;
751 Kreibich et al. 2009; Merz et al. 2010; Qi and Altinakar 2011b; 2011a; 2012; Ebrahimian, Gulliver,
752 and Wilson 2016; Ebrahimian et al. 2015). To gain a fuller picture of flood hazards, future research
753 should aim to develop ML models that can hindcast these additional flood characteristics. We also
754 focused on river maximum water depths and did not hindcast inundation on floodplains (out-of-
755 channel). Developing ML-based models that can satisfactorily hindcast out-of-channel maximum
756 water depths should be a focus of future research; the transferability of ML-based models for such
757 estimations should be also evaluated. High water marks (HWMs) can be used to train the model
758 for such hindcasting. However, HWMs are subject to large uncertainties (Schubert et al. 2022).
759 Therefore, one challenge in developing models that hindcast maximum water depths over
760 floodplains is the availability of reliable observations. Satellite-based observations are also often

761 limited to flood status data; maximum water depths cannot be estimated using these types of
762 datasets. Newly launched satellites, such as the Surface Water and Ocean Topography (SWOT)
763 mission, can provide additional data for such estimations.

764 As part of future work, it is also essential to consider the sensitivity of stream gauges to changes
765 in flow once water exceeds bankfull levels. This is significant as water height changes at a slower
766 rate beyond bankfull due to the compound channel shape. Wide floodplains can lead to similar
767 stage elevations for quite different flow conditions. This sensitivity assessment can offer insights
768 about whether water depths can be estimated once flood conditions are established, which has
769 implications for the model transferability across events.

770 We recommend that future work compares the performance of our ML-based model to
771 traditional physically-based and morphologic-based models using the same datasets. By evaluating
772 the performance, generalizability, and computational efficiency of our ML-based model versus
773 these traditional modeling approaches, we will be able to better validate the strengths of our data-
774 driven methodology. Detailed error analyses between the approaches can also reveal insights into
775 where additional physics knowledge needs to be incorporated into the ML-based model structure
776 and training to improve performance.

777 Thus, although we found ML-based models are transferable across flood events when informed
778 by relevant physical features at meaningful locations, there are still several areas that require
779 further investigations. By addressing these limitations, future research can corroborate our findings
780 about the performance and transferability of ML-based models in estimating maximum water
781 depths as computationally-efficient modeling frameworks.

782 5. Summary and conclusions

783 This paper developed an ML-based model for hindcast maximum water depths to address two
784 major limitations of past research in applying ML models for flood estimations: solely predicting
785 flood status (classification-based models) and debate on the transferability of these models across
786 events. We used ANN-MLP to hindcast maximum water depths over an event on a coastal
787 watershed, which is affected by fluvial and tidal floods. The model was informed by underlying
788 physical flood processes and initial conditions (in the watershed and rivers), represented through
789 a set of features (geographic location, topographic, climatic, land surface, hydrologic,
790 hydrodynamic and soil). Unlike previous applications of ML algorithms, our model estimated
791 maximum water depths by accounting for the spatial distribution of the processes through
792 considering both local contributions (at a given location) and those from the upstream watersheds.
793 We demonstrated the model on a HUC6 watershed, Lower Hudson, in the Northeastern United
794 States and evaluated its transferability across major flood events—Hurricanes Ida, Sandy, Irene
795 and Isaias. Feature selection techniques were used to identify the most influential features for flood
796 hindcast. Hyperparameter optimization was performed to fine-tune the ML model, and its
797 performance was evaluated using various metrics. The results showed that the model performed
798 satisfactorily in estimating maximum water depths for the original event, Hurricane Ida ($R^2= 0.94$,
799 $MAE= 0.64$ meters, $MDAE= 0.45$ meters, $NRMSE= 24\%$, and $F_Q= 138\%$). The model
800 transferability (i.e., applying the validated model as is without any additional parameter tuning)
801 within the same watershed against three other events showed that the developed model was
802 promising in the estimations ($R^2> 0.7$, $MAE< 1.71$ meters, $MDAE< 1.78$ meters, $NRMSE < 109\%$,
803 and $F_Q< 370\%$). This showed the model ability to capture complex relationships between the
804 maximum flood depth and pertinent features beyond what it was originally trained for. Future

805 research is needed to further evaluate the transferability of ML models across events and
806 watersheds with different drainage areas for flood depth estimations.

807 **Code availability**

808 The ML codes accessible at GitHub: ([https://github.com/mpakdehi/ANN_MLP-flood-depth-](https://github.com/mpakdehi/ANN_MLP-flood-depth-model)
809 [model](https://github.com/mpakdehi/ANN_MLP-flood-depth-model)).

810 **Data availability**

811 All the data are public domain and can be acquired from online repositories.

812 **Author contribution**

813 **MP:** Data curation, Formal analysis, Investigation, Methodology, Software, Validation,
814 Visualization, Writing – original draft preparation; **EA:** Conceptualization, Methodology, Funding
815 acquisition, Project administration, Supervision, Writing – review & editing; **BN:** Methodology,
816 Writing – review & editing; **EC:** Visualization, Writing – review & editing.

817 **Competing interests**

818 The authors declare that they have no conflict of interest.

819 **Acknowledgements**

820 This study was partially supported through a research grant by United States’ National Science
821 Foundation (award number 2203180). We thank Paul Bates for the detailed review and fruitful
822 comments on this manuscript.

823 **References**

824 Abdollahi, Abolfazl, and Biswajeet Pradhan. 2021. “Urban Vegetation Mapping from Aerial
825 Imagery Using Explainable AI (XAI).” *Sensors* 21 (14): 4738.
826 <https://doi.org/10.3390/s21144738>.
827 Abdrabo, Karim I., Sameh A. Kantoush, Aly Esmail, Mohamed Saber, Tetsuya Sumi, Mahmood
828 Almamari, Bahaa Elboshy, and Safaa Ghoniem. 2023. “An Integrated Indicator-Based
829 Approach for Constructing an Urban Flood Vulnerability Index as an Urban Decision-

830 Making Tool Using the PCA and AHP Techniques: A Case Study of Alexandria, Egypt.”
831 Urban Climate 48 (March): 101426. <https://doi.org/10.1016/j.uclim.2023.101426>.

832 Abrahart, Robert, P. E. Kneale, and Linda M. See. 2004. *Neural Networks for Hydrological*
833 *Modeling*. CRC Press.

834 Adamowski, Jan, Hiu Fung Chan, Shiv O. Prasher, and Vishwa Nath Sharda. 2011. “Comparison
835 of Multivariate Adaptive Regression Splines with Coupled Wavelet Transform Artificial
836 Neural Networks for Runoff Forecasting in Himalayan Micro-Watersheds with Limited
837 Data.” *Journal of Hydroinformatics* 14 (3): 731–44.
838 <https://doi.org/10.2166/hydro.2011.044>.

839 Agarap, Abien Fred. 2019. “Deep Learning Using Rectified Linear Units (ReLU).” arXiv.
840 <http://arxiv.org/abs/1803.08375>.

841 Ahmadisharaf Ebrahim, Camacho René A., Zhang Harry X., Hantush Mohamed M., and
842 Mohamoud Yusuf M. 2019. “Calibration and Validation of Watershed Models and
843 Advances in Uncertainty Analysis in TMDL Studies.” *Journal of Hydrologic Engineering*
844 24 (7): 03119001. [https://doi.org/10.1061/\(ASCE\)HE.1943-5584.0001794](https://doi.org/10.1061/(ASCE)HE.1943-5584.0001794).

845 Ahmadisharaf, Ebrahim, and Alfred J Kalyanapu. 2019. “A Coupled Probabilistic Hydrologic and
846 Hydraulic Modelling Framework to Investigate the Uncertainty of Flood Loss Estimates.”
847 *Journal of Flood Risk Management* 12 (S2): e12536. <https://doi.org/10.1111/jfr3.12536>.

848 Ahmadisharaf, Ebrahim, Alfred J. Kalyanapu, Jason R. Lillywhite, and Gina L. Tonn. 2018. “A
849 Probabilistic Framework to Evaluate the Uncertainty of Design Hydrograph: Case Study
850 of Swannanoa River Watershed.” *Hydrological Sciences Journal* 63 (12): 1776–90.
851 <https://doi.org/10.1080/02626667.2018.1525616>.

852 Allen, David M. 1974. “The Relationship Between Variable Selection and Data Augmentation and
853 a Method for Prediction.” *Technometrics* 16 (1): 125–27.
854 <https://doi.org/10.1080/00401706.1974.10489157>.

855 Anderson, Tiffany R., Charles H. Fletcher, Matthew M. Barbee, Bradley M. Romine, Sam Lemmo,
856 and Jade M. S. Delevaux. 2018. “Modeling Multiple Sea Level Rise Stresses Reveals up
857 to Twice the Land at Risk Compared to Strictly Passive Flooding Methods.” *Scientific*
858 *Reports* 8 (1): 14484. <https://doi.org/10.1038/s41598-018-32658-x>.

859 Bafitlhile, Thabo Michael, and Zhijia Li. 2019. “Applicability of ϵ -Support Vector Machine and
860 Artificial Neural Network for Flood Forecasting in Humid, Semi-Humid and Semi-Arid
861 Basins in China.” *Water* 11 (1): 85. <https://doi.org/10.3390/w11010085>.

862 Bales, J.d., and C.r. Wagner. 2009. “Sources of Uncertainty in Flood Inundation Maps.” *Journal*
863 *of Flood Risk Management* 2 (2): 139–47. [https://doi.org/10.1111/j.1753-](https://doi.org/10.1111/j.1753-318X.2009.01029.x)
864 [318X.2009.01029.x](https://doi.org/10.1111/j.1753-318X.2009.01029.x).

865 Bates, Paul D. 2022. “Flood Inundation Prediction.” *Annual Review of Fluid Mechanics* 54 (1):
866 287–315. <https://doi.org/10.1146/annurev-fluid-030121-113138>.

867 Bates, Paul D., Richard J. Dawson, Jim W. Hall, Matthew S. Horritt, Robert J. Nicholls, Jon Wicks,
868 and Mohamed Ahmed Ali Mohamed Hassan. 2005. “Simplified Two-Dimensional
869 Numerical Modelling of Coastal Flooding and Example Applications.” *Coastal*
870 *Engineering* 52 (9): 793–810. <https://doi.org/10.1016/j.coastaleng.2005.06.001>.

871 Berkahn, Simon, Lothar Fuchs, and Insa Neuweiler. 2019. “An Ensemble Neural Network Model
872 for Real-Time Prediction of Urban Floods.” *Journal of Hydrology* 575 (August): 743–54.
873 <https://doi.org/10.1016/j.jhydrol.2019.05.066>.

- 874 Beven II, John L., Andrew Hagen, and Robbie Berg. 2022. "Tropical Cyclone Report -
875 HURRICANE IDA (AL092021)." National Hurricane Center. April 4, 2022.
876 https://www.nhc.noaa.gov/data/tcr/AL092021_Ida.pdf.
- 877 Beven, K. J., and M. J. Kirkby. 1979. "A Physically Based, Variable Contributing Area Model of
878 Basin Hydrology / Un Modèle à Base Physique de Zone d'appel Variable de l'hydrologie
879 Du Bassin Versant." *Hydrological Sciences Bulletin* 24 (1): 43–69.
880 <https://doi.org/10.1080/02626667909491834>.
- 881 Bhuyian, Md N. M., and Alfred Kalyanapu. 2020. "Predicting Channel Conveyance and
882 Characterizing Planform Using River Bathymetry via Satellite Image Compilation
883 (RiBaSIC) Algorithm for DEM-Based Hydrodynamic Modeling." *Remote Sensing* 12
884 (17): 2799. <https://doi.org/10.3390/rs12172799>.
- 885 Blake, Eric S., Todd B. Kimberlain, Robert J. Berg, John P. Cangialosi, and John L. Beven II.
886 2013. "Tropical Cyclone Report - Hurricane Sandy (AL182012)." National Hurricane
887 Center. February 12, 2013. https://www.nhc.noaa.gov/data/tcr/AL182012_Sandy.pdf.
- 888 Bottou, Léon. 2012. "Stochastic Gradient Descent Tricks." In *Neural Networks: Tricks of the
889 Trade*, edited by Grégoire Montavon, Geneviève B. Orr, and Klaus-Robert Müller,
890 7700:421–36. Lecture Notes in Computer Science. Berlin, Heidelberg: Springer Berlin
891 Heidelberg. https://doi.org/10.1007/978-3-642-35289-8_25.
- 892 Cao, Yifan, Hongliang Jia, Junnan Xiong, Weiming Cheng, Kun Li, Quan Pang, and Zhiwei Yong.
893 2020. "Flash Flood Susceptibility Assessment Based on Geodetector, Certainty Factor, and
894 Logistic Regression Analyses in Fujian Province, China." *ISPRS International Journal of
895 Geo-Information* 9 (12): 748. <https://doi.org/10.3390/ijgi9120748>.
- 896 Chang, Li-Chiu, Jia-Yi Liou, and Fi-John Chang. 2022. "Spatial-Temporal Flood Inundation
897 Nowcasts by Fusing Machine Learning Methods and Principal Component Analysis."
898 *Journal of Hydrology* 612 (September): 128086.
899 <https://doi.org/10.1016/j.jhydrol.2022.128086>.
- 900 Chen, Yuguo, Xinyi Zhang, Kejun Yang, Shiyi Zeng, and Anyu Hong. 2023. "Modeling Rules of
901 Regional Flash Flood Susceptibility Prediction Using Different Machine Learning
902 Models." *Frontiers in Earth Science* 11.
903 <https://www.frontiersin.org/articles/10.3389/feart.2023.1117004>.
- 904 Costabile, Pierfranco, Carmelina Costanzo, and Francesco Macchione. 2017. "Performances and
905 Limitations of the Diffusive Approximation of the 2-d Shallow Water Equations for Flood
906 Simulation in Urban and Rural Areas." *Applied Numerical Mathematics, New Trends in
907 Numerical Analysis: Theory, Methods, Algorithms and Applications (NETNA 2015)*, 116
908 (June): 141–56. <https://doi.org/10.1016/j.apnum.2016.07.003>.
- 909 Dawson, C. W., R. J. Abrahart, A. Y. Shamseldin, and R. L. Wilby. 2006. "Flood Estimation at
910 Ungauged Sites Using Artificial Neural Networks." *Journal of Hydrology* 319 (1): 391–
911 409. <https://doi.org/10.1016/j.jhydrol.2005.07.032>.
- 912 Dixit, A, S Sahany, B Rajagopalan, and S Choubey. 2022. "Role of Changing Land Use and Land
913 Cover (LULC) on the 2018 Megafloods over Kerala, India." *Climate Research* 89
914 (October): 1–14. <https://doi.org/10.3354/cr01701>.
- 915 Ebrahimian, Ali, Abdollah Ardeshir, Iman Zahedi Rad, and Seyyed Hassan Ghodsypour. 2015.
916 "Urban Stormwater Construction Method Selection Using a Hybrid Multi-Criteria
917 Approach." *Automation in Construction* 58 (October): 118–28.
918 <https://doi.org/10.1016/j.autcon.2015.07.014>.

- 919 Ebrahimian, Ali, John S. Gulliver, and Bruce N. Wilson. 2016. “Effective Impervious Area for
920 Runoff in Urban Watersheds: EIA in Urban Watersheds.” *Hydrological Processes* 30 (20):
921 3717–29. <https://doi.org/10.1002/hyp.10839>.
- 922 Elkharchy, Ismail. 2022. “Flash Flood Water Depth Estimation Using SAR Images, Digital
923 Elevation Models, and Machine Learning Algorithms.” *Remote Sensing* 14 (3): 440.
924 <https://doi.org/10.3390/rs14030440>.
- 925 Fereshtehpour, Mohammad, Mostafa Esmailzadeh, Reza Saleh Alipour, and Steven J. Burian.
926 2024. “Impacts of DEM Type and Resolution on Deep Learning-Based Flood Inundation
927 Mapping.” *Earth Science Informatics* 17 (2): 1125–45. [https://doi.org/10.1007/s12145-](https://doi.org/10.1007/s12145-024-01239-0)
928 [024-01239-0](https://doi.org/10.1007/s12145-024-01239-0).
- 929 Fernández-Pato, Javier, Daniel Caviedes-Voullième, and Pilar García-Navarro. 2016.
930 “Rainfall/Runoff Simulation with 2D Full Shallow Water Equations: Sensitivity Analysis
931 and Calibration of Infiltration Parameters.” *Journal of Hydrology* 536 (May): 496–513.
932 <https://doi.org/10.1016/j.jhydrol.2016.03.021>.
- 933 Gallegos, Humberto A., Jochen E. Schubert, and Brett F. Sanders. 2012. “Structural Damage
934 Prediction in a High-Velocity Urban Dam-Break Flood: Field-Scale Assessment of
935 Predictive Skill.” *Journal of Engineering Mechanics* 138 (10): 1249–62.
936 [https://doi.org/10.1061/\(ASCE\)EM.1943-7889.0000427](https://doi.org/10.1061/(ASCE)EM.1943-7889.0000427).
- 937 Geisser, Seymour. 1975. “The Predictive Sample Reuse Method with Applications.” *Journal of*
938 *the American Statistical Association* 70 (350): 320–28.
939 <https://doi.org/10.1080/01621459.1975.10479865>.
- 940 Gray W. Brunner. 2016. “HEC-RAS, River Analysis System Hydraulic Reference Manual.”
941 February 2016. [https://www.hec.usace.army.mil/software/hec-ras/documentation/HEC-](https://www.hec.usace.army.mil/software/hec-ras/documentation/HEC-RAS%205.0%20Reference%20Manual.pdf)
942 [RAS%205.0%20Reference%20Manual.pdf](https://www.hec.usace.army.mil/software/hec-ras/documentation/HEC-RAS%205.0%20Reference%20Manual.pdf).
- 943 Gudiyangada Nachappa, Thimmaiah, Sepideh Tavakkoli Piralilou, Khalil Gholamnia, Omid
944 Ghorbanzadeh, Omid Rahmati, and Thomas Blaschke. 2020. “Flood Susceptibility
945 Mapping with Machine Learning, Multi-Criteria Decision Analysis and Ensemble Using
946 Dempster Shafer Theory.” *Journal of Hydrology* 590 (November): 125275.
947 <https://doi.org/10.1016/j.jhydrol.2020.125275>.
- 948 Guo, Zifeng, João P. Leitão, Nuno E. Simões, and Vahid Moosavi. 2021. “Data-Driven Flood
949 Emulation: Speeding up Urban Flood Predictions by Deep Convolutional Neural
950 Networks.” *Journal of Flood Risk Management* 14 (1): e12684.
951 <https://doi.org/10.1111/jfr3.12684>.
- 952 Horel, Enguerrand, and Kay Giesecke. 2019. “Computationally Efficient Feature Significance and
953 Importance for Machine Learning Models.” <https://doi.org/10.48550/ARXIV.1905.09849>.
- 954 Hosseini, Farzaneh Sajedi, Bahram Choubin, Amir Mosavi, Narjes Nabipour, Shahaboddin
955 Shamshirband, Hamid Darabi, and Ali Torabi Haghghi. 2020. “Flash-Flood Hazard
956 Assessment Using Ensembles and Bayesian-Based Machine Learning Models: Application
957 of the Simulated Annealing Feature Selection Method.” *Science of The Total Environment*
958 711 (April): 135161. <https://doi.org/10.1016/j.scitotenv.2019.135161>.
- 959 Hosseiny, Hossein, Foad Nazari, Virginia Smith, and C. Nataraj. 2020. “A Framework for
960 Modeling Flood Depth Using a Hybrid of Hydraulics and Machine Learning.” *Scientific*
961 *Reports* 10 (1): 8222. <https://doi.org/10.1038/s41598-020-65232-5>.
- 962 Hu, Anson, and Ibrahim Demir. 2021. “Real-Time Flood Mapping on Client-Side Web Systems
963 Using HAND Model.” *Hydrology* 8 (2): 65. <https://doi.org/10.3390/hydrology8020065>.

964 Huang, Faming, Siyu Tao, Deying Li, Zhipeng Lian, Filippo Catani, Jinsong Huang, Kailong Li,
965 and Chuhong Zhang. 2022. “Landslide Susceptibility Prediction Considering
966 Neighborhood Characteristics of Landslide Spatial Datasets and Hydrological Slope Units
967 Using Remote Sensing and GIS Technologies.” *Remote Sensing* 14 (18): 4436.
968 <https://doi.org/10.3390/rs14184436>.

969 Jafarzadegan, Keighobad, and Venkatesh Merwade. 2019. “Probabilistic Floodplain Mapping
970 Using HAND-Based Statistical Approach.” *Geomorphology* 324 (January): 48–61.
971 <https://doi.org/10.1016/j.geomorph.2018.09.024>.

972 Jafarzadegan, Keighobad, Hamid Moradkhani, Florian Pappenberger, Hamed Moftakhari, Paul
973 Bates, Peyman Abbaszadeh, Reza Marsooli, et al. 2023. “Recent Advances and New
974 Frontiers in Riverine and Coastal Flood Modeling.” *Reviews of Geophysics* 61 (2):
975 e2022RG000788. <https://doi.org/10.1029/2022RG000788>.

976 Jiang, Junguang, Yang Shu, Jianmin Wang, and Mingsheng Long. 2024. “Transferability in Deep
977 Learning: A Survey.” *Ar5iv*. 2024. <https://ar5iv.labs.arxiv.org/html/2201.05867>.

978 Joseph, V. Roshan. 2022. “Optimal Ratio for Data Splitting.” *Statistical Analysis and Data Mining:
979 The ASA Data Science Journal* 15 (4): 531–38. <https://doi.org/10.1002/sam.11583>.

980 Kalyanapu, Alfred J., Siddharth Shankar, Eric R. Pardyjak, David R. Judi, and Steven J. Burian.
981 2011. “Assessment of GPU Computational Enhancement to a 2D Flood Model.”
982 *Environmental Modelling & Software* 26 (8): 1009–16.
983 <https://doi.org/10.1016/j.envsoft.2011.02.014>.

984 Karamouz, Mohammad, Reza Saleh Alipour, Mahnoor Roohinia, and Mohammad Fereshtehpour.
985 2022. “A Remote Sensing Driven Soil Moisture Estimator: Uncertain Downscaling With
986 Geostatistically Based Use of Ancillary Data.” *Water Resources Research* 58 (10):
987 e2022WR031946. <https://doi.org/10.1029/2022WR031946>.

988 Khosravi, Khabat, Binh Thai Pham, Kamran Chapi, Ataollah Shirzadi, Himan Shahabi, Inge
989 Revhaug, Indra Prakash, and Dieu Tien Bui. 2018. “A Comparative Assessment of
990 Decision Trees Algorithms for Flash Flood Susceptibility Modeling at Haraz Watershed,
991 Northern Iran.” *Science of The Total Environment* 627 (June): 744–55.
992 <https://doi.org/10.1016/j.scitotenv.2018.01.266>.

993 Kim, Sooyoul, Yoshiharu Matsumi, Shunqi Pan, and Hajime Mase. 2016. “A Real-Time Forecast
994 Model Using Artificial Neural Network for after-Runner Storm Surges on the Tottori
995 Coast, Japan.” *Ocean Engineering* 122 (August): 44–53.
996 <https://doi.org/10.1016/j.oceaneng.2016.06.017>.

997 Kreibich, H., K. Piroth, I. Seifert, H. Maiwald, U. Kunert, J. Schwarz, B. Merz, and A. H. Thielen.
998 2009. “Is Flow Velocity a Significant Parameter in Flood Damage Modelling?” *Natural
999 Hazards and Earth System Sciences* 9 (5): 1679–92. <https://doi.org/10.5194/nhess-9-1679-2009>.

1000

1001 Kulp, Scott A., and Benjamin H. Strauss. 2019. “New Elevation Data Triple Estimates of Global
1002 Vulnerability to Sea-Level Rise and Coastal Flooding.” *Nature Communications* 10 (1):
1003 4844. <https://doi.org/10.1038/s41467-019-12808-z>.

1004 Kundzewicz, ZW, Buda Su, Yanjun Wang, Jun Xia, Jinlong Huang, and Tong Jiang. 2019. “Flood
1005 Risk and Its Reduction in China.” *Advances in Water Resources* 130 (August): 37–45.
1006 <https://doi.org/10.1016/j.advwatres.2019.05.020>.

1007 Latto, Andy, Andrew Hagen, and Robbie Berg. 2021. "Tropical Cyclone Report - HURRICANE
1008 ISAIAS (AL092020)." National Hurricane Center. June 11, 2021.
1009 https://www.nhc.noaa.gov/data/tcr/AL092020_Isaias.pdf.

1010 Lee, Deuk-Hwan, Yun-Tae Kim, and Seung-Rae Lee. 2020. "Shallow Landslide Susceptibility
1011 Models Based on Artificial Neural Networks Considering the Factor Selection Method and
1012 Various Non-Linear Activation Functions." *Remote Sensing* 12 (7): 1194.
1013 <https://doi.org/10.3390/rs12071194>.

1014 Lixion A., Avila, and John Cangialosi. 2013. "Tropical Cyclone Report - Hurricane Irene
1015 (AL092011)." National Hurricane Center. April 11, 2013.
1016 https://www.nhc.noaa.gov/data/tcr/AL092011_Irene.pdf.

1017 Löwe, Roland, Julian Böhm, David Getreuer Jensen, Jorge Leandro, and Søren Højmark
1018 Rasmussen. 2021. "U-FLOOD – Topographic Deep Learning for Predicting Urban Pluvial
1019 Flood Water Depth." *Journal of Hydrology* 603 (December): 126898.
1020 <https://doi.org/10.1016/j.jhydrol.2021.126898>.

1021 Lundberg, Scott, and Su-In Lee. 2017. "A Unified Approach to Interpreting Model Predictions."
1022 arXiv. <http://arxiv.org/abs/1705.07874>.

1023 Macedo, Francisco, M. Rosário Oliveira, António Pacheco, and Rui Valadas. 2019. "Theoretical
1024 Foundations of Forward Feature Selection Methods Based on Mutual Information."
1025 *Neurocomputing* 325 (January): 67–89. <https://doi.org/10.1016/j.neucom.2018.09.077>.

1026 McCulloch, Warren S., and Walter Pitts. 1943. "A Logical Calculus of the Ideas Immanent in
1027 Nervous Activity." *The Bulletin of Mathematical Biophysics* 5 (4): 115–33.
1028 <https://doi.org/10.1007/BF02478259>.

1029 Merwade, Venkatesh, Francisco Olivera, Mazdak Arabi, and Scott Edleman. 2008. "Uncertainty
1030 in Flood Inundation Mapping: Current Issues and Future Directions." *Journal of
1031 Hydrologic Engineering* 13 (7): 608–20. [https://doi.org/10.1061/\(ASCE\)1084-
1032 0699\(2008\)13:7\(608\)](https://doi.org/10.1061/(ASCE)1084-0699(2008)13:7(608)).

1033 Merz, B, Heidi Kreibich, R Schwarze, and Annette Thielen. 2010. "Review Article" Assessment
1034 of Economic Flood Damage". *Natural Hazards and Earth System Sciences* 10: 1697–
1035 1724. <https://doi.org/10.5194/nhess-10-1697-2010>.

1036 Ming, Xiaodong, Qihua Liang, Xilin Xia, Dingmin Li, and Hayley J. Fowler. 2020. "Real-Time
1037 Flood Forecasting Based on a High-Performance 2-D Hydrodynamic Model and
1038 Numerical Weather Predictions." *Water Resources Research* 56 (7): e2019WR025583.
1039 <https://doi.org/10.1029/2019WR025583>.

1040 Mishra, Ashok, Sourav Mukherjee, Bruno Merz, Vijay P. Singh, Daniel B. Wright, Villarini
1041 Gabriele, Subir Paul, et al. 2022. "An Overview of Flood Concepts, Challenges, and Future
1042 Directions." *Journal of Hydrologic Engineering* 27 (6).
1043 [https://ascelibrary.org/doi/full/10.1061/\(ASCE\)HE.1943-5584.0002164](https://ascelibrary.org/doi/full/10.1061/(ASCE)HE.1943-5584.0002164).

1044 National Hurricane Center. 2022. "National Hurricane Center." 2022.
1045 <https://www.nhc.noaa.gov/index.shtml>.

1046 Nguyen, Quang Hung, Hai-Bang Ly, Lanh Si Ho, Nadhir Al-Ansari, Hiep Van Le, Van Quan Tran,
1047 Indra Prakash, and Binh Thai Pham. 2021. "Influence of Data Splitting on Performance of
1048 Machine Learning Models in Prediction of Shear Strength of Soil." *Mathematical Problems
1049 in Engineering* 2021 (February): e4832864. <https://doi.org/10.1155/2021/4832864>.

1050 NOAA. 2023. "NOAA Tides & Currents." CO-OPS Map - NOAA Tides & Currents. 2023.
1051 <https://tidesandcurrents.noaa.gov/map/index.html>.

1052 NOAA's NCEI. 2022. "Data Search | National Centers for Environmental Information (NCEI)."
1053 2022. <https://www.ncei.noaa.gov/access/search/data-search/local-climatological-data>.

1054 Park, Man Ho, Munsol Ju, and Jae Young Kim. 2020. "Bayesian Approach in Estimating Flood
1055 Waste Generation: A Case Study in South Korea." *Journal of Environmental Management*
1056 265 (July): 110552. <https://doi.org/10.1016/j.jenvman.2020.110552>.

1057 Pham, Binh Thai, Chinh Luu, Tran Van Phong, Phan Trong Trinh, Ataollah Shirzadi, Somayeh
1058 Renoud, Shahrokh Asadi, Hiep Van Le, Jason von Meding, and John J. Clague. 2021. "Can
1059 Deep Learning Algorithms Outperform Benchmark Machine Learning Algorithms in
1060 Flood Susceptibility Modeling?" *Journal of Hydrology* 592 (January): 125615.
1061 <https://doi.org/10.1016/j.jhydrol.2020.125615>.

1062 Pradhan, Biswajeet. 2009. "Journal of Spatial Hydrology Vol.9, No.2 Fall 2009."

1063 Qi, Honghai, and Mustafa S. Altinakar. 2011a. "A Conceptual Framework of Agricultural Land
1064 Use Planning with BMP for Integrated Watershed Management." *Journal of*
1065 *Environmental Management* 92 (1): 149–55.
1066 <https://doi.org/10.1016/j.jenvman.2010.08.023>.

1067 ———. 2011b. "Vegetation Buffer Strips Design Using an Optimization Approach for Non-Point
1068 Source Pollutant Control of an Agricultural Watershed." *Water Resources Management* 25
1069 (2): 565–78. <https://doi.org/10.1007/s11269-010-9714-9>.

1070 ———. 2012. "GIS-Based Decision Support System for Dam Break Flood Management under
1071 Uncertainty with Two-Dimensional Numerical Simulations." *Journal of Water Resources*
1072 *Planning and Management* 138 (4): 334–41. [https://doi.org/10.1061/\(ASCE\)WR.1943-5452.0000192](https://doi.org/10.1061/(ASCE)WR.1943-5452.0000192).

1074 Rafiei-Sardooi, Elham, Ali Azareh, Bahram Choubin, Amir H. Mosavi, and John J. Clague. 2021.
1075 "Evaluating Urban Flood Risk Using Hybrid Method of TOPSIS and Machine Learning."
1076 *International Journal of Disaster Risk Reduction* 66 (December): 102614.
1077 <https://doi.org/10.1016/j.ijdrr.2021.102614>.

1078 Rahmati, Omid, Hamid Reza Pourghasemi, and Hossein Zeinivand. 2016. "Flood Susceptibility
1079 Mapping Using Frequency Ratio and Weights-of-Evidence Models in the Golastan
1080 Province, Iran." *Geocarto International* 31 (1): 42–70.
1081 <https://doi.org/10.1080/10106049.2015.1041559>.

1082 Reckien, Diana. 2018. "What Is in an Index? Construction Method, Data Metric, and Weighting
1083 Scheme Determine the Outcome of Composite Social Vulnerability Indices in New York
1084 City." *Regional Environmental Change* 18 (5): 1439–51. <https://doi.org/10.1007/s10113-017-1273-7>.

1086 Rennó, Camilo Daleles, Antonio Donato Nobre, Luz Adriana Cuartas, João Viane Soares, Martin
1087 G. Hodnett, Javier Tomasella, and Maarten J. Waterloo. 2008. "HAND, a New Terrain
1088 Descriptor Using SRTM-DEM: Mapping Terra-Firme Rainforest Environments in
1089 Amazonia." *Remote Sensing of Environment* 112 (9): 3469–81.
1090 <https://doi.org/10.1016/j.rse.2008.03.018>.

1091 Rezaie, Fatemeh, Mahdi Panahi, Sayed M. Bateni, Changhyun Jun, Christopher M. U. Neale, and
1092 Saro Lee. 2022. "Novel Hybrid Models by Coupling Support Vector Regression (SVR)
1093 with Meta-Heuristic Algorithms (WOA and GWO) for Flood Susceptibility Mapping."
1094 *Natural Hazards* 114 (2): 1247–83. <https://doi.org/10.1007/s11069-022-05424-6>.

- 1095 Rumelhart, David E., James L. McClelland, and PDP Research Group. 1986. *Parallel Distributed*
 1096 *Processing: Explorations in the Microstructure of Cognition: Foundations*. The MIT Press.
 1097 <https://doi.org/10.7551/mitpress/5236.001.0001>.
- 1098 Salvati, Aryan, Alireza Moghaddam Nia, Ali Salajegheh, Kayvan Ghaderi, Dawood Talebpour
 1099 Asl, Nadhir Al-Ansari, Feridon Solaimani, and John J. Clague. 2023. "Flood Susceptibility
 1100 Mapping Using Support Vector Regression and Hyper-Parameter Optimization." *Journal*
 1101 *of Flood Risk Management* n/a (n/a): e12920. <https://doi.org/10.1111/jfr3.12920>.
- 1102 Schubert, Jochen E., Adam Luke, Amir AghaKouchak, and Brett F. Sanders. 2022. "A Framework
 1103 for Mechanistic Flood Inundation Forecasting at the Metropolitan Scale." *Water Resources*
 1104 *Research* 58 (10): e2021WR031279. <https://doi.org/10.1029/2021WR031279>.
- 1105 Schubert, Jochen E., and Brett F. Sanders. 2012. "Building Treatments for Urban Flood Inundation
 1106 Models and Implications for Predictive Skill and Modeling Efficiency." *Advances in Water*
 1107 *Resources* 41 (June): 49–64. <https://doi.org/10.1016/j.advwatres.2012.02.012>.
- 1108 Sheridan, Scott C., Cameron C. Lee, Ryan E. Adams, Erik T. Smith, Douglas E. Pirhalla, and Varis
 1109 Ransibrahmanakul. 2019. "Temporal Modeling of Anomalous Coastal Sea Level Values
 1110 Using Synoptic Climatological Patterns." *Journal of Geophysical Research: Oceans* 124
 1111 (9): 6531–44. <https://doi.org/10.1029/2019JC015421>.
- 1112 Singarimbun, Roy Nuary, Erna Budhiarti Nababan, and Opim Salim Sitompul. 2019. "Adaptive
 1113 Moment Estimation To Minimize Square Error In Backpropagation Algorithm." In 2019
 1114 *International Conference of Computer Science and Information Technology*
 1115 *(ICoSNIKOM)*, 1–7. Medan, Indonesia: IEEE.
 1116 <https://doi.org/10.1109/ICoSNIKOM48755.2019.9111563>.
- 1117 Sridhar, Venkataramana, Syed Azhar Ali, and David J. Sample. 2021. "Systems Analysis of
 1118 Coupled Natural and Human Processes in the Mekong River Basin." *Hydrology* 8 (3): 140.
 1119 <https://doi.org/10.3390/hydrology8030140>.
- 1120 Stone, M. 1974. "Cross-Validatory Choice and Assessment of Statistical Predictions." *Journal of*
 1121 *the Royal Statistical Society: Series B (Methodological)* 36 (2): 111–33.
 1122 <https://doi.org/10.1111/j.2517-6161.1974.tb00994.x>.
- 1123 Stow, Craig A., Chris Roessler, Mark E. Borsuk, James D. Bowen, and Kenneth H. Reckhow.
 1124 2003. "Comparison of Estuarine Water Quality Models for Total Maximum Daily Load
 1125 Development in Neuse River Estuary." *Journal of Water Resources Planning and*
 1126 *Management* 129 (4): 307–14. [https://doi.org/10.1061/\(ASCE\)0733-9496\(2003\)129:4\(307\)](https://doi.org/10.1061/(ASCE)0733-9496(2003)129:4(307)).
- 1128 Sun, Deliang, Jiahui Xu, Haijia Wen, and Yue Wang. 2020. "An Optimized Random Forest Model
 1129 and Its Generalization Ability in Landslide Susceptibility Mapping: Application in Two
 1130 Areas of Three Gorges Reservoir, China." *Journal of Earth Science* 31 (6): 1068–86.
 1131 <https://doi.org/10.1007/s12583-020-1072-9>.
- 1132 Teng, J., A.J. Jakeman, J. Vaze, B.F.W. Croke, D. Dutta, and S. Kim. 2017. "Flood Inundation
 1133 Modelling: A Review of Methods, Recent Advances and Uncertainty Analysis." *Environmental*
 1134 *Modelling & Software* 90 (April): 201–16.
 1135 <https://doi.org/10.1016/j.envsoft.2017.01.006>.
- 1136 Trottier, Ludovic, Philippe Giguere, and Brahim Chaib-draa. 2017. "Parametric Exponential
 1137 Linear Unit for Deep Convolutional Neural Networks." In 2017 16th IEEE International
 1138 *Conference on Machine Learning and Applications (ICMLA)*, 207–14. Cancun, Mexico:
 1139 IEEE. <https://doi.org/10.1109/ICMLA.2017.00038>.

1140 USGS. 2022. “TNM Download V2.” 2022. <https://apps.nationalmap.gov/downloader/>.

1141 Viglione, Alberto, Giuliano Di Baldassarre, Luigia Brandimarte, Linda Kuil, Gemma Carr, José
 1142 Luis Salinas, Anna Scolobig, and Günter Blöschl. 2014. “Insights from Socio-Hydrology
 1143 Modelling on Dealing with Flood Risk – Roles of Collective Memory, Risk-Taking
 1144 Attitude and Trust.” *Journal of Hydrology, Creating Partnerships Between Hydrology and
 1145 Social Science: A Priority for Progress*, 518 (October): 71–82.
 1146 <https://doi.org/10.1016/j.jhydrol.2014.01.018>.

1147 Wagenaar, Dennis, Stefan Lüdtkke, Kai Schröter, Laurens M. Bouwer, and Heidi Kreibich. 2018.
 1148 “Regional and Temporal Transferability of Multivariable Flood Damage Models.” *Water
 1149 Resources Research* 54 (5): 3688–3703. <https://doi.org/10.1029/2017WR022233>.

1150 Wan Jaafar, Wan Zurina, and Dawei Han. 2012. “Uncertainty in Index Flood Modelling Due to
 1151 Calibration Data Sizes.” *Hydrological Processes* 26 (2): 189–201.
 1152 <https://doi.org/10.1002/hyp.8135>.

1153 Wang, Jie, Qihong Tang, Xiaobo Yun, Aifang Chen, Siao Sun, and Dai Yamazaki. 2022. “Flood
 1154 Inundation in the Lancang-Mekong River Basin: Assessing the Role of Summer
 1155 Monsoon.” *Journal of Hydrology* 612 (September): 128075.
 1156 <https://doi.org/10.1016/j.jhydrol.2022.128075>.

1157 Wang, Zhaoli, Chengguang Lai, Xiaohong Chen, Bing Yang, Shiwei Zhao, and Xiaoyan Bai.
 1158 2015. “Flood Hazard Risk Assessment Model Based on Random Forest.” *Journal of
 1159 Hydrology* 527 (August): 1130–41. <https://doi.org/10.1016/j.jhydrol.2015.06.008>.

1160 Wenger, Seth J., and Julian D. Olden. 2012. “Assessing Transferability of Ecological Models: An
 1161 Underappreciated Aspect of Statistical Validation.” *Methods in Ecology and Evolution* 3
 1162 (2): 260–67. <https://doi.org/10.1111/j.2041-210X.2011.00170.x>.

1163 Youssef, Ahmed M., Biswajeet Pradhan, Abhirup Dikshit, and Ali M. Mahdi. 2022. “Comparative
 1164 Study of Convolutional Neural Network (CNN) and Support Vector Machine (SVM) for
 1165 Flood Susceptibility Mapping: A Case Study at Ras Gharib, Red Sea, Egypt.” *Geocarto
 1166 International* 37 (26): 11088–115. <https://doi.org/10.1080/10106049.2022.2046866>.

1167 Zahura, Faria T., Jonathan L. Goodall, Jeffrey M. Sadler, Yawen Shen, Mohamed M. Morsy, and
 1168 Madhur Behl. 2020. “Training Machine Learning Surrogate Models From a High-Fidelity
 1169 Physics-Based Model: Application for Real-Time Street-Scale Flood Prediction in an
 1170 Urban Coastal Community.” *Water Resources Research* 56 (10).
 1171 <https://doi.org/10.1029/2019WR027038>.

1172 Zhang, Fang, Xiaolin Zhu, and Desheng Liu. 2014. “Blending MODIS and Landsat Images for
 1173 Urban Flood Mapping.” *International Journal of Remote Sensing* 35 (9): 3237–53.
 1174 <https://doi.org/10.1080/01431161.2014.903351>.

1175 Zhao, Gang, Bo Pang, Zongxue Xu, Dingzhi Peng, and Depeng Zuo. 2020. “Urban Flood
 1176 Susceptibility Assessment Based on Convolutional Neural Networks.” *Journal of
 1177 Hydrology* 590 (November): 125235. <https://doi.org/10.1016/j.jhydrol.2020.125235>.

1178 Zheng, Xing, David G. Tarboton, David R. Maidment, Yan Y. Liu, and Paola Passalacqua. 2018.
 1179 “River Channel Geometry and Rating Curve Estimation Using Height above the Nearest
 1180 Drainage.” *JAWRA Journal of the American Water Resources Association* 54 (4): 785–
 1181 806. <https://doi.org/10.1111/1752-1688.12661>.

1182 Zhu, D., Q. Ren, Y. Xuan, Y. Chen, and I. D. Cluckie. 2013. “An Effective Depression Filling
 1183 Algorithm for DEM-Based 2-D Surface Flow Modelling.” *Hydrology and Earth System
 1184 Sciences* 17 (2): 495–505. <https://doi.org/10.5194/hess-17-495-2013>.

1185 Zhu, Jun-Jie, Meiqi Yang, and Zhiyong Jason Ren. 2023. "Machine Learning in Environmental
1186 Research: Common Pitfalls and Best Practices." *Environmental Science & Technology*,
1187 June. <https://doi.org/10.1021/acs.est.3c00026>.
1188